EXPERIMENTAL AND NUMERICAL ASSESSMENT OF SAMPLE HETEROGENEITY ON TRIAXIAL FAILURE MECHANISM USING CHROME STEEL SPHERICAL PARTICLES

A Thesis

by

TAM NGUYEN MINH DUONG

Submitted to the Office of Graduate and Professional Studies of
Texas A&M University
in partial fulfillment of the requirements for the degree of

MASTER OF SCIENCE

Chair of Committee,	Zenon Medina-Cetina
Committee Members,	Ivan Damnjanovic
	Eduardo Gildin
Head of Department,	Robin Autenrieth

December 2015

Major Subject: Civil Engineering

ABSTRACT

Previous studies have shown that sample preparation techniques used to reconstruct specimens for granular materials can have substantial influence on theirs mechanistic behavior. Since the Distinct Element Method (DEM) becomes popular for modeling multi-physics problems using granular materials, the homogeneity of reconstituted samples should be investigated and accurately characterized in order to have consistent modeling results. The air-pluviation method was used to reconstitute samples composed of a homogeneous granular material at different density conditions. Then, selected samples were taken to perform triaxial compression tests in order to obtain the global strength behavior of the specimen under compression loading. X-ray computed tomography (CT) and image analysis techniques were later used to characterize the spatial particle structure of a sample. The sample preparation method and compression test were modeled numerically using discrete element method via a program called PFC3D from ITASCA. The microstructure of the numerical sample was compared to the results of the image analysis to determine if the heterogeneity of the sample could be accurately replicated in DEM by measuring void ratio of the reconstituted samples. In addition, the engineering response of numerical sample under compression was also compared with experimental results. Experimental results showed the sample heterogeneity was affected by sample preparation conditions thus influenced on its stress-strain response when subjected to triaxial compression. Although direct comparison of spatial void ratio between the experimental samples and the numerical models was not obtained, the comparison of

spatial void ratio of the numerical models created by air pluviation method and radius expansion method showed that the void ratio of samples prepared by air pluviation method had lower percentage error with the global experimental void ratio. Due to time limitation, only four numerical simulations of triaxial compression were performed.

DEDICATION

To my dearest Mother,

Nguyen Thi My Dung

I am grateful to be your daughter

Thank you for everything

I love and miss you so much

R.I.P.

ACKNOWLEDGEMENTS

I would like to express my gratitude to the people who have significant impacts to my study which leads to the completion of this thesis.

Firstly, I am sincerely appreciate my advisor, Dr. Medina-Cetina, for his incredible support and guidance throughout the work. His continuous encouragement to improve my work influenced me both in research and in life to always try for better results. I have learnt many lessons to be applied not only in research but also in life from his experience and leadership. It has been my pleasure to work with him since my undergraduate research. I also thank him for being patience and compassion for me during the hardest time of my life.

I would like to thank Dr. Damnjanovic and Dr. Gildin, for being a part of my committee and for being very responsive to my questions.

I would like to thank my parents, family members and friends for their support and encouragement. Especially I thank my parents for their continuous support and encouragement despite the distance.

I would also like to thank Lucy Hatherill and Luis Mayo for helping to complete the experiment portions of this study, including sample preparation and triaxial compression tests.

I would like to thank Mike Linger for his guidance and helping to set up the required laboratory equipment needed for this study.

I would like to thank ITASCA for their help and guidance with PFC3D.

TABLE OF CONTENTS

Page

LIST OF FIGURES

Page

LIST OF TABLES

Page

CHAPTER I

INTRODUCTION

Previous studies has shown sample preparation techniques significant influence the engineering responses of soils samples [1-8]. Soils samples constituted in the laboratory are assumed to be homogeneous but they are in fact heterogeneous. Therefore, the heterogeneity of the samples would have influence to the material response when subjected to different laboratory tests, and also contribute to the failure mechanism of the samples. The use of Distinct Element Model (DEM) technique via PFC3D from Itasca has become popular for many research disciplines such as geology, civil engineering, mining, agriculture, pharmaceuticals [9-16]. Originally developed by Cundall and Strack in the 1970's, DEM is known for the capability of reproducing particles interactions for large deformations [17]. Improving the understanding of the micro-mechanical behavior of granular materials with respect to meso- and macro- mechanical applications is currently a pressing need in geotechnical engineering. Preceding studies combined digital image correlation and DEM techniques with experimental testing results to obtain a better understanding of micro-mechanical behavior of different materials [18-25]. This research is oriented towards the characterization of the heterogeneity for granular materials (e.g. chrome steel spheres) samples subjected to large deformations during triaxial compression tests by the use of X-rays computed tomography (CT) and DEM modeling using PFC3D for material response prediction. The objective is to accurately replicate the non-

homogenous condition of reconstituted samples using DEM in PFC3D, thus obtain the stress-strain response of heterogeneous samples to compare with laboratory results.

1.1 Motivation

The study on the behaviors of granular materials has always been an important topic in geotechnical engineering field, focusing on how the materials flow, deform and their corresponding failure mechanisms [26]. Accurately modelling the behaviors of granular materials will allow engineers to predict or assess possible landslides, slope stability, settlement of foundations on granular media, and so on. Proper risk assessment on geomaterial responses helps prevent and minimize tragic structural consequences but still remain cost-effective. Unlike the traditional finite-element method (FEM) used to predict behavior of geomaterials by discretizing the media into a mesh that the displacement and rotation of each component are dependent to each other, the discrete-element method (DEM) allows its components (disks, spheres, or clumps) to displace and rotate independently to each other [18]. DEM is promising to solve large deformation problems which require intensive computational effort using FEM. This study will investigate the ability to replicate the heterogeneity of the sample using DEM for different sample formation techniques, as well as comparing the stress-strain response of sample subjected to triaxial compression. The result of this study will generates the macro-micro properties of granular materials to predict their behaviors for large deformation problems like deep water cone penetration test.

1.2 Sample Preparation Methods

Numerous studies have shown that engineering properties of granular materials can be greatly influenced by the method to reconstitute sample under control conditions. Moist tamping, dry funnel deposition, water pluviation and air pluviation are common techniques to reconstitute samples. All of these techniques aim to replicate a uniform sample to simulate in-situ condition. Although the void ratio of samples prepared by different techniques is almost identical to each other, the behaviors of the samples are greatly reliant on the method of reconstitution samples. Initially, Oda [1] and Arthur and Menzies [2] found that the stress-strain relationship of sand depends strongly on the sample preparation techniques. Ladd [3] observed that preparation methods significantly affect the cyclic shear strength of sand. Similarly, studies of Mulislis et al. [4] reported the effects of sample preparation techniques to the liquefaction characteristics of sand subjected to cyclic loadings. Abouzar Sadrekarimi and Scott M. Olson [5] investigated the effect of specimen preparation method on critical state behavior of sand. Viad et al. [6] recommended water pluviation method over moist tamping method as samples prepared by the water pluviation method showed dilative behavior while samples prepared by the moist tamping method showed liquefaction behavior when subjected to triaxial compression and extension tests. Yamamuro et al. [7] pointed out that samples prepared by pluviated methods tend to have more stable grain-to-grain contacts, which resulted in a stable behavior, compared to dry funnel deposition and slurry deposition methods. Thomson and Wong's study [8] showed that both water pluviation and moist tamping methods resulted in non-homogenous samples. However, void ratio of water pluviated

sample was lower only at the top quarter of the sample height while void ratio of moist tamped sample varied along the sample height.

1.3 Distinct Element Method Applications in PFC

There have been numerous studies on geo-material behaviors using distinct element method (DEM) in Particle Flow Code (PFC3D) since the program was first established by Itasca in 1996. The results of the numerical simulations aim to provide an appropriate macroscopic mechanical behavior as comparison to the laboratory experiments in order to predict the failure mechanism of the materials.

Zhu et al. [27] presents a review in DEM theory developments over the past decades which focuses on particle models for the calculation of the particle–particle and particle–fluid interaction, coupling to describe particle–fluid flow, and available techniques for incorporating DEM to continuum modeling. A detailed list of DEM studies and applications is provided by Zhu et al. [28]. Zhu's paper categorizes DEM studies in to three areas, which are particle packing (cohesionless and cohesive particles), particle flow (confined and unconfined flow) and particle-fluid flow (cohesionless and cohesive particles).

O'Sullivan's review of the use of DEM in geomechanics presents a general overview for people whom are unfamiliar with using DEM in research practice [29]. Her paper presents a brief summary of DEM evolution, types of particles, calculation algorithms, post-processing and general approach to validate and calibrate a DEM model. According to O'Sullivan, DEM simulations of geo-materials include cohesionless soil, cemented

sand, rock, and clay. Simulations of granular materials, both uncemented and cemented, are common in resembling the behaviors of sand and rock while simulations of clay are less common due to the complexity of the particle's surface force and particle's geometry. O'Sullivan also composes a list of key studies based on different types of physical tests such as biaxial compression tests, triaxial and true triaxial tests, plane strain tests, simple shear tests, direct shear tests, interface shear tests, machine, penetration, and arching at field scale. O'Sullivan points out potential area for future DEM studies are to incorporate DEM to industrial or field scale problems, as well as to increase accuracy in particle morphology and mechanical response (improve current contact constitutive models).

1.4 Problem Statement

Noble [25] conducted a study on the heterogeneity of specimens due to sample preparation techniques using both X-rays computed tomography and DEM. In his study, both dry funnel deposition and air pluviation methods were used to reconstitute samples from loosest density to highest density. The result showed a reduction trend in sample void ratio as the drop height increased. However, there was variation in the void ratio between experiment and numerical simulation. This was thought to be caused experimental setup and human factors that effected the constitution of sample. The reproducibility of the sample preparation was a major challenge. Also, there were only one sample taken CT scan images and three samples taken triaxial compression test. Therefore partial information about the influence of sample preparation techniques to the global material behavior under compression was obtained.

This study aims to complete the study started by Noble by improving the experimental technique for sample preparation, taking CT scan images for each condition reconstituting the sample, performing triaxial compression test for each condition the sample is reconstituted and replicating the compression tests in PFC3D.

1.5 Hypothesis

Samples composed of granular materials generated following standard procedures for homogeneous samples show heterogeneous structures [25]. Sample heterogeneity can influence the engineering response of a granular material. The heterogeneity of the sample can be reproduced for numerical simulations by modeling the sample preparation method. A method can be developed to investigate the relation between microstructure formation and global behavior of granular materials using X-rays computed tomography and discrete element modeling.

1.6 Thesis Outline

Chapter II introduces the sample preparation method chosen for this study, which is air pluviation method. Videos capturing the air pluviation process are used to analyze the velocity of the spheres as they enter the acrylic tube. The choice of material to be used in this study is also discussed. Chapter III presents the procedure for triaxial compression test, as well as the test result. Chapter IV introduces the used of X-rays computed tomography (CT) scans of the prepared samples and image processing techniques, to identify the center of the spheres and reconstruction of the images for further analysis.

Chapter V presents the theoretical framework of DEM in PFC3D including the calculation cycle and contact constitute models. It follows a discussion on two procedures to prepare samples, the radius expansion method and the air pluviation method. The triaxial compression simulation settings are also discussed. Chapter VI introduces different methods to obtain spatial void ratio including PFC measurement spheres, planar void ratio variation and regional void ratio of a plan. Chapter VII summarizes and discusses the results from previous chapters and presents ideas for future study.

CHAPTER II

SAMPLE PREPARATION

2.1 Material Description

Spheres of the same diameter are used to represent homogenous granular material in this study. The choice material to study the behavior of granular materials is significantly important due to the fact that the behavior of granular materials are influenced by grain size distribution, particle shape, surface friction, void ratio of the sample and preparation methods. For the purpose of this study, to investigate the effect of sample preparation methods on the behavior of granular materials, other factors that affect the behavior of granular material are minimized by the choice of material of same size, spherical shape and low surface friction coefficient. Several materials are taken into consideration such as: chrome steel, silicon nitride, titanium, and polycarbonate plastic. According to the manufacturer, Thomson Precision Balls, properties of each material are listed on Table 1 [30]. O'Sullivan previous study provided engineering properties of steel spheres: shear modulus of 7.9×10^{10} Pa, Poisson's ratio of 0.28, and the sphere boundary coefficient of 0.228 and 0.06 for sphere-wall contact and sphere-sphere contact respectively [21]. In addition, the cost of chrome steel spheres are the second lowest among four materials. The decision of material is also based on Noble's study [25]. Therefore, chrome steel spheres, in the size of 3-millimeter and 6-millimeter diameter respectively, are used in this study since they minimize the effect of deformation and friction between each other, and they are also cost effective.

Table 1: Mechanical Properties of Available Spherical Materials

Properties	Material			
	Chrome Steel	Titanium	Silicon Nitride	Polycarbonate Plastic
Density (kg/m^3)	7,833	4,510	3,190	1,200
Tensile strength (MPa)	2,240	434	830	62
Shear modulus (MPa)	80,000	44,000	130,000	786
Young's Modulus (MPa)	205,000	116,000	310,000	2,760
Friction coefficient	0.228	0.3	0.7	0.24

2.2 Air Pluviation Method

For the purpose of this study, the specimen preparation process is a very important task, which is hypothesized that would condition the failure mechanisms found in triaxial tests on granular specimens. The main goal is to produce a uniformly distributed cylindrical specimen using a homogenous particle material. The air pluviation method is chosen to reconstitute samples as this method is commonly used to create homogenous samples for varying void ratios, as recommended from Noble's study [25].

In order to prepare a homogenous cylindrical specimen, the air pluviation sample preparation method was used. Air pluviation reconstitutes soil particles by drizzling of soil particles through a set of diffuser meshes placed on top of a fall tube. Figure 1 presents the set-up of equipment during sample preparation process. A frame made of PVC tubes is built to hold the funnel in place, preventing the fluctuation of the funnel while composing sample.

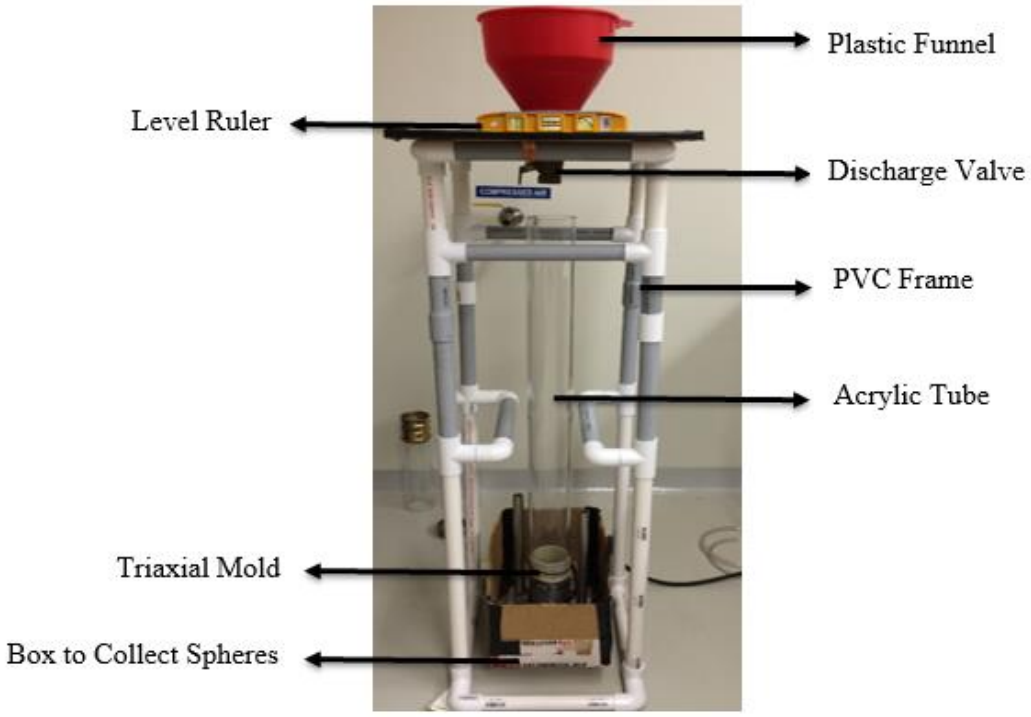

Figure 1: Sample Preparation Equipment Set-up.

The fall tube that has the same diameter of the mold rested below prevents the dispersion of the rain and obtains a uniform concentration of rain across the diameter. The mold is fastened using two hoop clamps. Pressure is applied on the mold to keep the membrane in contact with the mold using a small vacuum pump. Sieves are placed on top of the tube to distribute the particle flow across the planar area. A plastic funnel is placed about 2.54 centimeter (one inch) above the sieve to control the flow of the particles. Steel particles are poured into the funnel while its end is being closed. Then they are allowed to settle before a one-inch- diameter valve, installed at the funnel's end, is opened. Spheres flow through the funnel, enter the meshes and are redistributed through the acrylic vertical

tube to densely form in the mold. Figure 2 presents the constituted sample when the mold is removed and subjected to 55 kPa confining pressure.

Figure 2: Constituted Sample Subjected to 55 kPa Confining Pressure

With a constant flow velocity, a denser state of the specimen can be archived by increasing the tube height. The fall height is varied from 30.48 centimeter (one foot) to 91.44 centimeter (three-foot-height). The number of sieves placed on top of the tube is also varied from zero sieve to three sieves. For reproducibility condition, five trials of each height are made and the dimensions and weight of each sample are recorded. The record of each steel specimen is used to generate a distribution of drop height versus void ratio

and the number of sieves versus void ratio of a homogenous particle material. Figure 3 presents the condition variation for air pluviation process. Table 2 presents the experimental design for sample preparation using air pluviation method. A step by step sample preparation procedure using air pluviation method is provided in the Appendix.

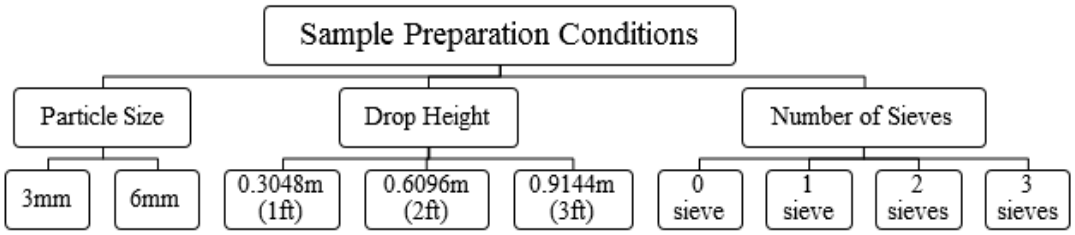

Figure 3: Sample Preparation Conditions.

Table 2: Experimental Design of Sample Preparation Using Air Pluviation Method

Experimental Framework			
3 mm diameter spheres		6 mm diameter spheres	
Number of sieves	Drop height, ft	Number of sieves	Drop height, ft
0; 1; 2; 3	1; 2; 3	0; 1; 2; 3	1; 2; 3

2.3 Flow of Particles Velocity Determination

Videos of the sample preparation process are captured and analyzed to ensure the flow velocity of particles are similar for each condition. A video analysis and modeling tool, Tracker [31], is used to analyze the motion of the spheres to obtain the sphere velocity based on kinematics equations for free fall. Due to the rapid falling of the spheres, the auto track feature of the program cannot be used, therefore, a manual selection of individual particle is conducted. At first, when the video capturing the air pluviation process is

loaded, the coordinate axes is set at the opening of the valve with origin is at the center of the opening. A calibration stick is established by setting the length of the stick equal to the width of the acrylic tube of 0.08825 m. Then, locations of 5 spheres are manually specified as the spheres entering the tube and free falling for a distance of approximately 0.15 m (0.5 ft). The velocity and acceleration of the spheres are calculated by the program so the sphere acceleration can be checked if it is equal to gravitational acceleration. Firgure 4 shows how the sphere velocity is obtain by Tracker. The measured sphere velocity can be checked with the velocity calculated by the kinematic equation:

$$v_f^2 = v_i^2 + 2a\Delta y$$

where v_i is initial velocity and $v_i = 0$; a is sphere acceleration and $a = g = -9.81\,\text{m/s}^2$; Δy is traveled distance of the sphere and $\Delta y = -0.1524\,\text{m}$.

By solving the equation, the sphere velocity should be approximately 1.73 m/s as it falls about 0.15 m into the acrylic tube. Finally, the first order statistics of the sphere velocity are calculated as well.

A summary of flow velocity is shown in Figure 5. The sphere velocity varies from 1.5 to 2.05 m/s with average velocity of 1.7 to 1.8 m/s. The average sphere velocity is closed to the theoretical velocity of 1.73 m/s. The variation might be due to inaccurate locating the sphere positions in the video that leads to inaccurate sphere velocity. Another possibility is that the spheres hit the edge of the tube as they fall so their velocity might be effected. The acceleration of spheres are obtained as well. Figure 6 shows sphere acceleration according to its velocity. The average acceleration is about 9.65 m/s^2 which is slightly below the gravitational acceleration of 9.81 m/s^2. The difference in acceleration

is thought to be a consequence of the error in measuring the sphere locations. Due to the fact that 3mm diameter spheres are too small to specify their positions using Tracker, only videos of 6mm diameter spheres are analyzed to get sphere velocity and acceleration.

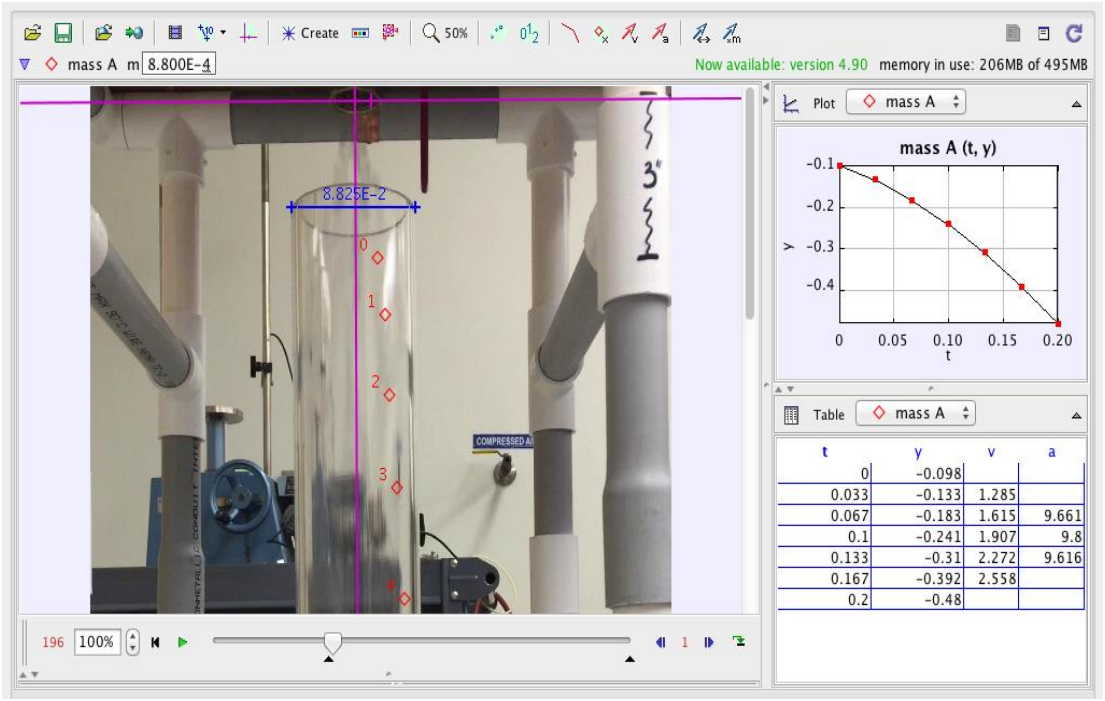

Figure 4: Analysis of Spheres Motion on Tracker.

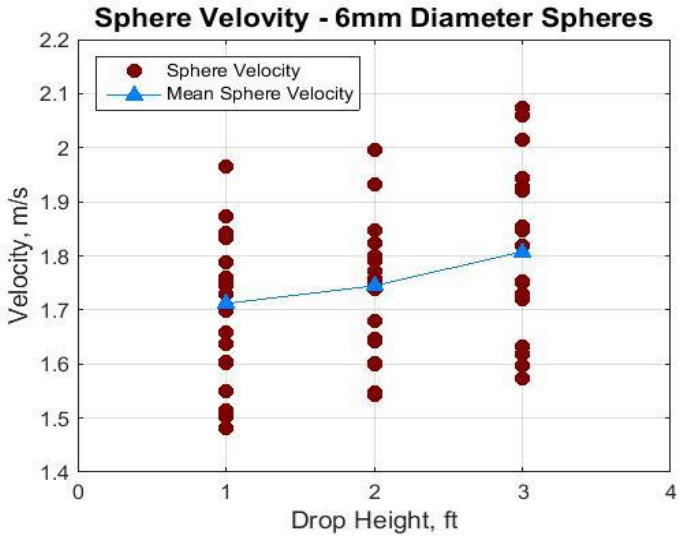

Figure 5: Sphere Velocity for the First 0.15 m of Free Fall.

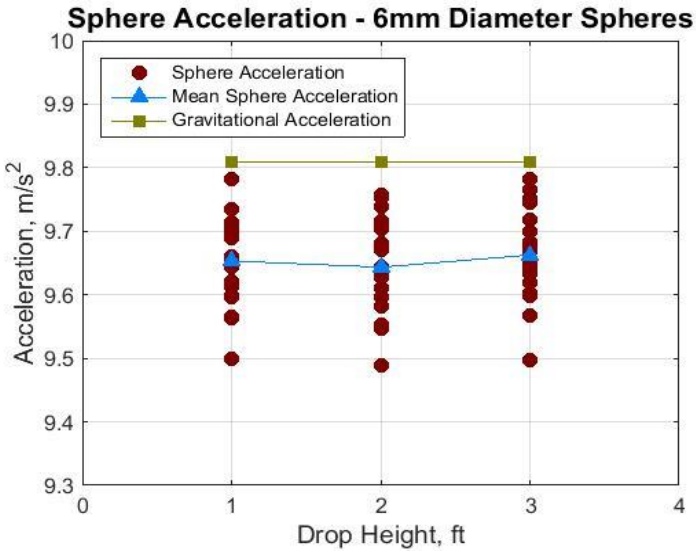

Figure 6: Sphere Acceleration for the First 0.15m of Free Fall.

2.4 Void Ratio Determination

As described before, five samples are prepared for each sample preparation condition. The global void ratio of the sample is obtained by the following steps. At first, dimensions

of each sample (height and diameter) and sample weight are recorded. Then, the void ratio is calculated using the formula:

$$e = \frac{V_V}{V_S} = \frac{V_V}{V_T - V_V}$$

where e is void ratio; V_T is total sample volume and $V_T = \pi H \frac{D^2}{4}$ where H and D are measured sample height and diameter; V_S is solid volume and $V_S = \frac{W_S}{\rho}$ where W_S is sample weight and ρ is sphere density; V_V is volume of void.

2.5 Results

For each sample reconstituted, the void ratio of the sample is calculated. Average void ratio is calculated for each condition the samples are prepared. Plots of void ratio are presented in Figure 7 to Figure 11 below for both sphere sizes with respect to drop height and number of sieves.

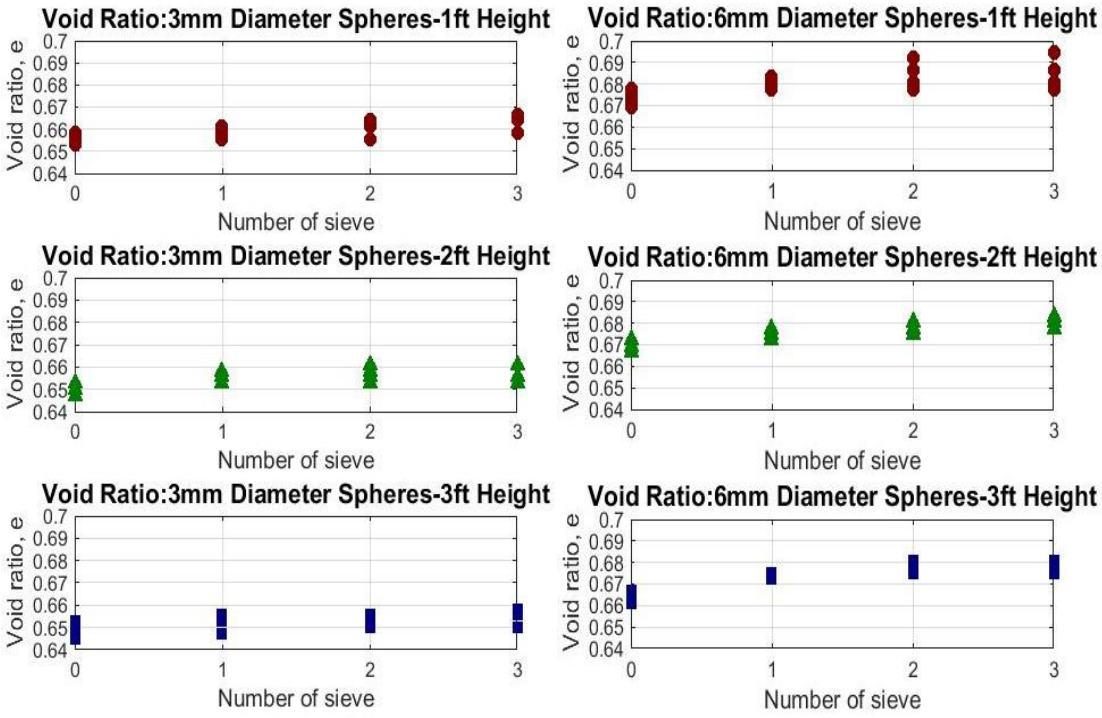

Figure 7: Void Ratio of 3 mm and 6 mm Diameter Sphere Samples versus Number of Sieves.

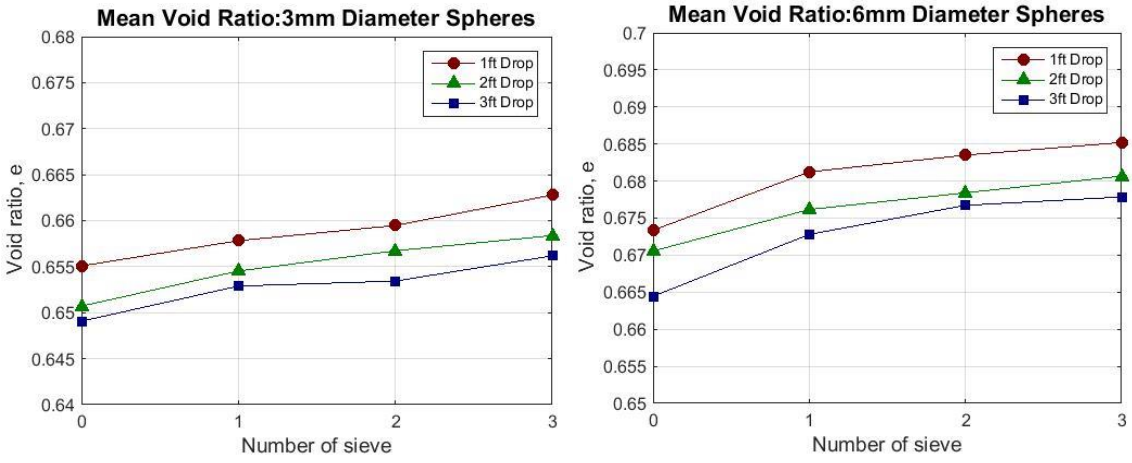

Figure 8: Mean Void Ratio of 3 mm and 6 mm Samples versus Number of Sieves.

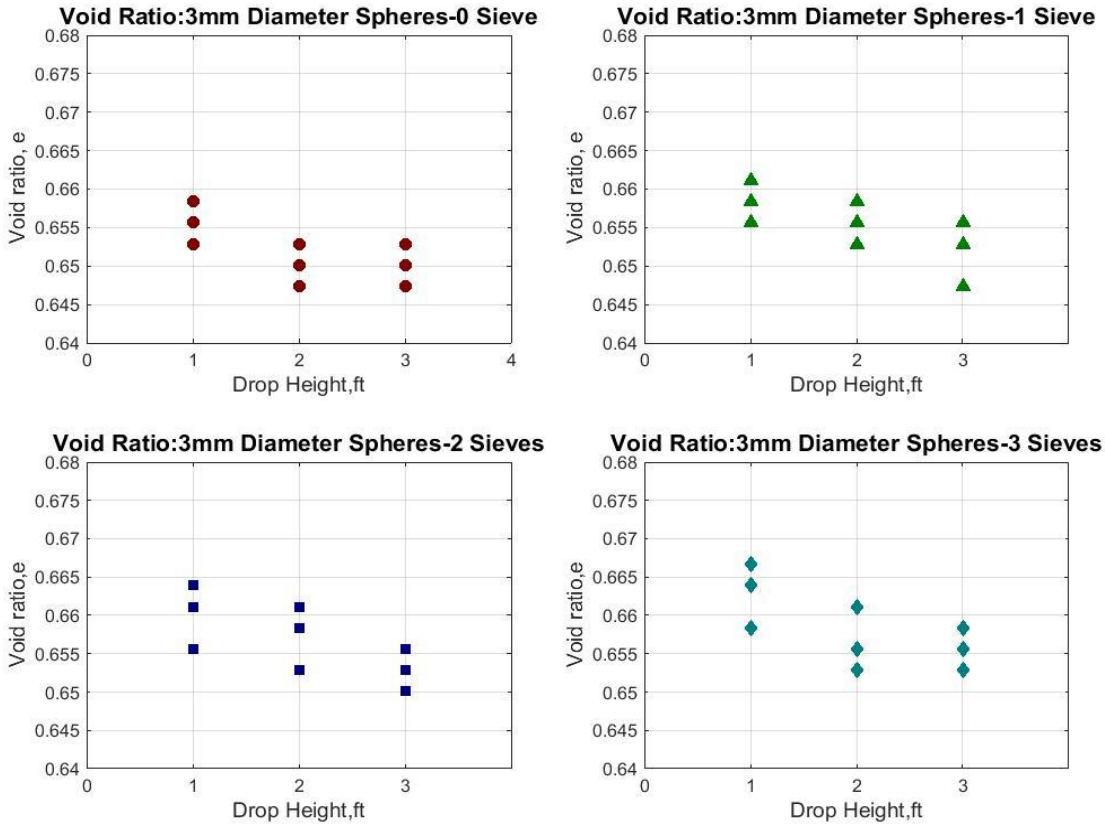

Figure 9: Void Ratio of 3 mm Diameter Spheres Samples versus Drop Height.

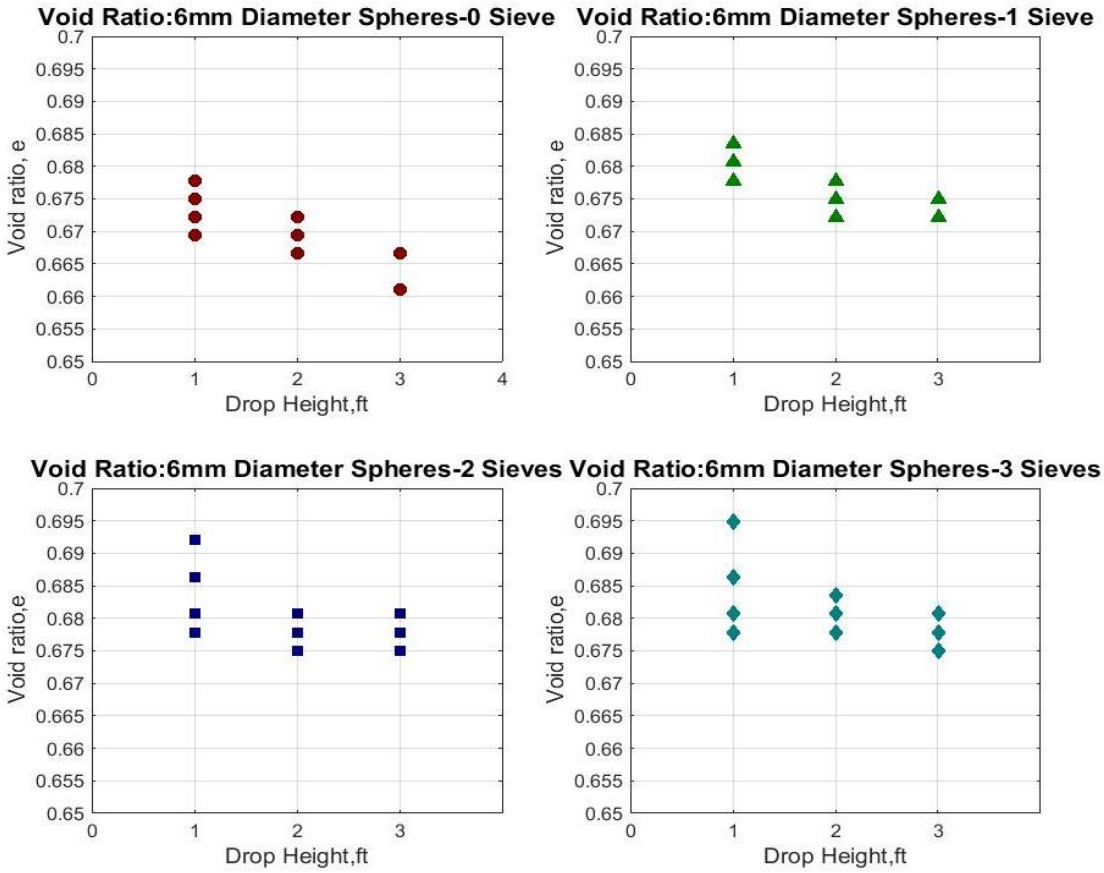

Figure 10: Void Ratio of 6 mm Diameter Spheres Samples versus Drop Height.

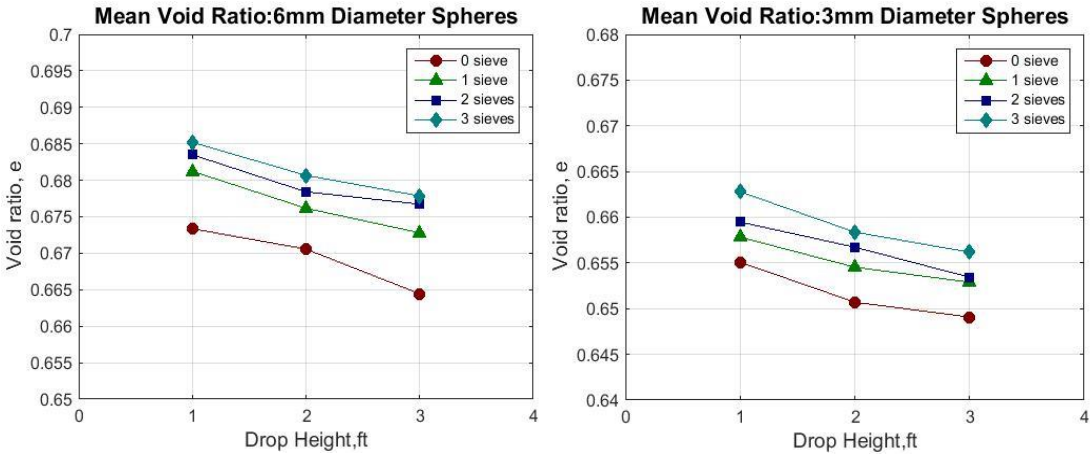

Figure 11: Mean Void Ratio of 3 mm and 6 mm Samples versus Drop Height.

In general, the sample void ratio tends to decrease as the drop height increases which means the sample is denser due to higher potential energy. The void ratio of samples prepared at the same drop height increases as more sieves are placed which means the sphere potential energy is reduced by contacting with the sieves that leads to lessen density state of the sample. Plots of sample void ratio shows the trend as predicted before. Three dimension plots of sample void ratio versus drop height and number of sieves are also presented in Figure 12 and Figure 13 for better understanding the correlation between those variables. Table 3 summarizes mean void ratio of samples made of 3 mm and 6 mm diameter spheres based on experiment framework.

Table 3: Mean Void Ratio of Samples for Both Sphere Sizes

Mean void ratio, e							
3 mm diameter spheres				6 mm diameter spheres			
Number of sieves	Drop height, ft			Number of sieves	Drop height, ft		
	1	2	3		1	2	3
0	0.6551	0.6507	0.6491	0	0.6734	0.6706	0.6644
1	0.6578	0.6545	0.6529	1	0.6812	0.6762	0.6728
2	0.6595	0.6567	0.6534	2	0.6835	0.6784	0.6767
3	0.6628	0.6584	0.6562	3	0.6852	0.6807	0.6779

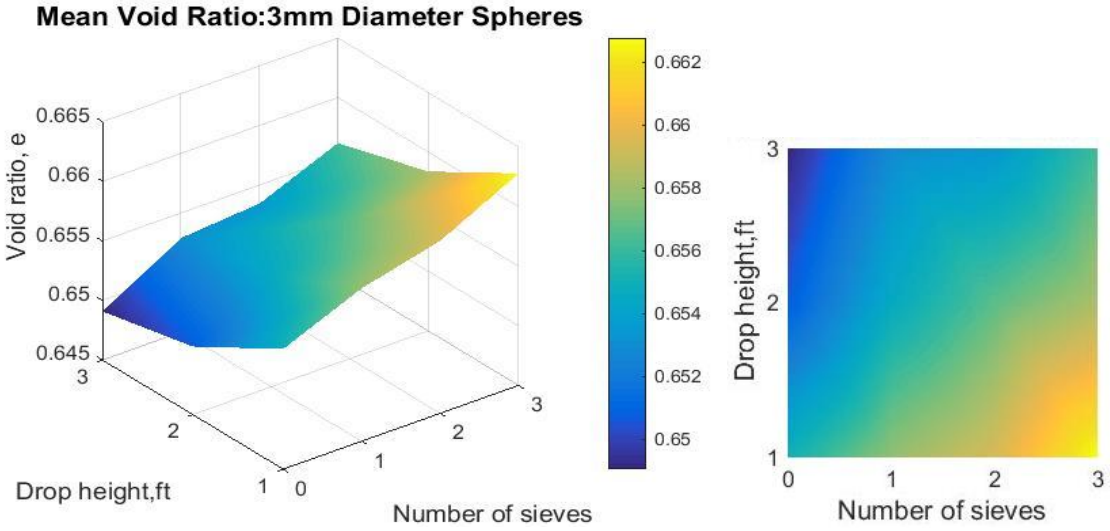

Figure 12: 3D Plot of Mean Void Ratio for 3mm Diameter Sphere Samples.

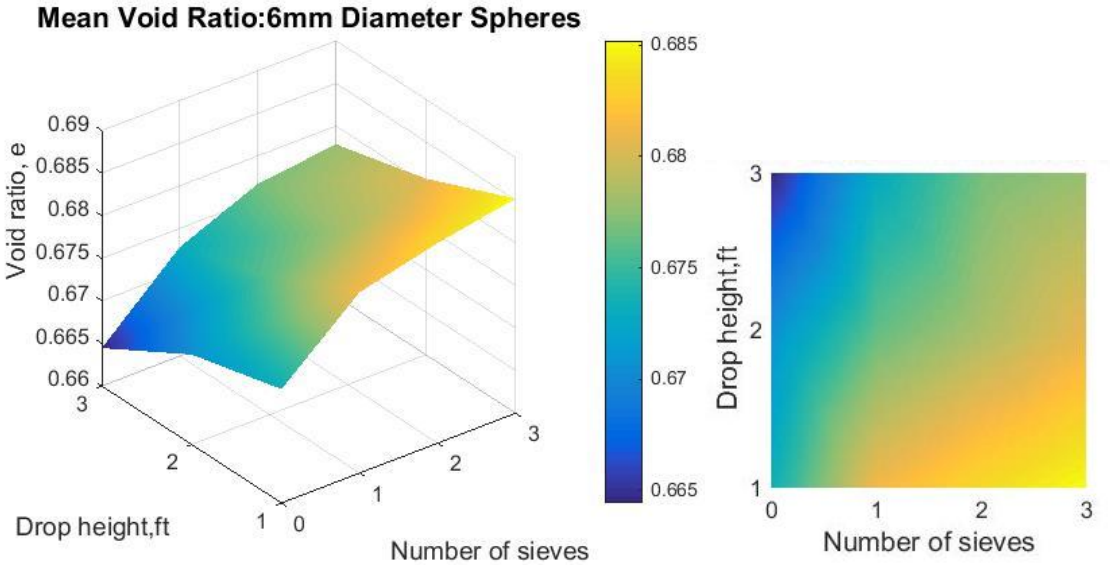

Figure 13: 3D Plot of Mean Void Ratio for 6mm Diameter Sphere Samples.

CHAPTER III

TRIAXIAL COMPRESSION TESTS

3.1 Test Procedure

A triaxial compression test is performed based on samples made out of steel spheres, as a way to obtain shear strength parameters of particles measuring the axial stress and axial strain of the specimen [32]. The ASTM standard procedure for the triaxial compression test is followed. The specimen is prepared as stated above and placed into the triaxial cell. Figure 14 shows the prepared sample being subjected to triaxial compression.

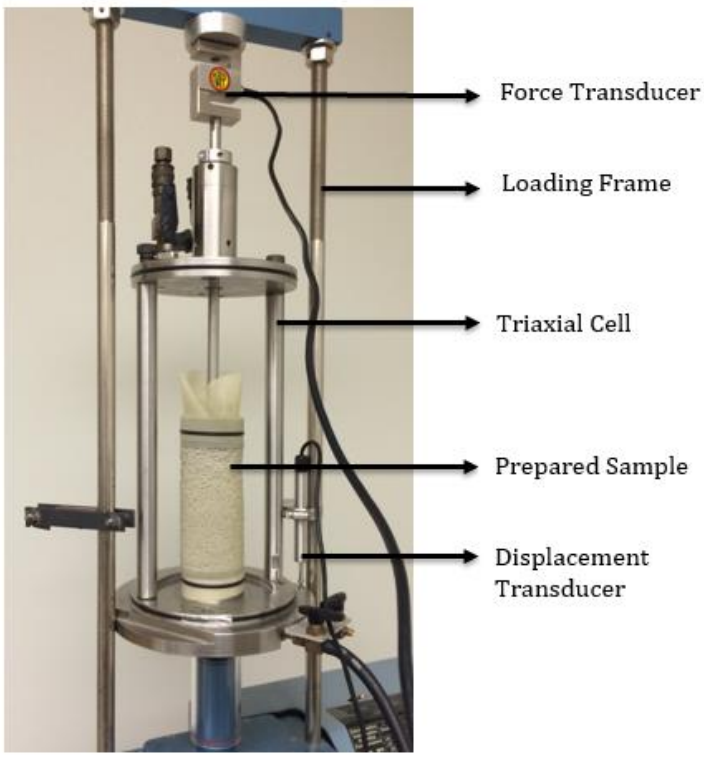

Figure 14: Prepared Specimen Subjected to Triaxial Compression.

A confining pressure of about 55 kPa has been applied to the specimen using vacuum pump since the specimen is prepared. A force transducer attached to a piston resting on the sample is used to capture the resistance of the specimen during shearing. The cell is then placed in the loading frame that connected to a displacement transducer. Both transducers are connected to the computer through a data acquisition device. The test starts as the loading frame is raised up at a rate of 1.6 millimeter per minute, while the confining pressure is still applied to the specimen. In other words, the strain rate of the triaxial test is 1.6 millimeter per minute. The transducers transfer the recorded data to the computer and by the use of LabView program [33], which uses measured voltages from the transducers to get the displacement and force applied to the specimen. The end result provides adequate data to determine the strength and deformation properties of a sample composed of steel particles. One triaxial compression test is performed for each condition the sample is prepared. The axial strain is obtained by the following equation:

$$\varepsilon = \frac{\Delta l}{l_0}$$

where ε is axial strain; Δl is the change in sample height; and l_0 is the original sample height.

The deviatoric stress is the difference between the major and minor principal stresses, obtained by the equation:

$$\sigma_1 - \sigma_3 = \frac{P}{A_c}$$

where σ_1 is the major principal stress; σ_3 is the minor principal stress also known as confining pressure; P is load applied to the sample; A_c is the current cross section of the sample which is calculated as $A_c = \frac{A_i}{(1-\varepsilon)}$, where A_i is the original cross section area of the sample.

3.2 Undrained Shear Strength

One sample for each condition constituted samples is subjected to triaxial compression test. Plots of deviatoric stress versus axial strain corresponding to sample void ratio for both sphere sizes are showed in Figure 15 to Figure 20 below.

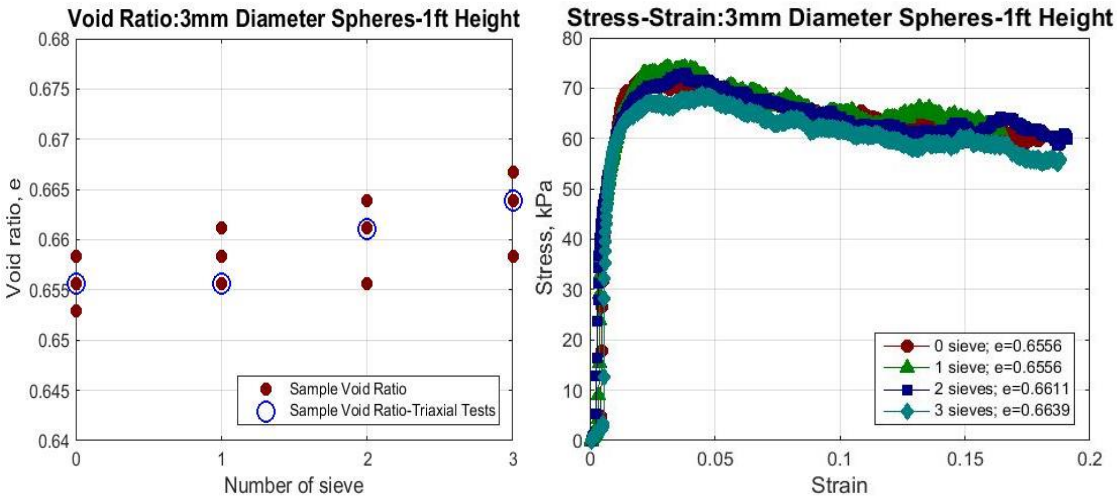

Figure 15: Stress-Strain Curves of Random 3 mm Diameter Sphere Samples Prepared at 1 ft Drop Height Subjected to Triaxial Compression.

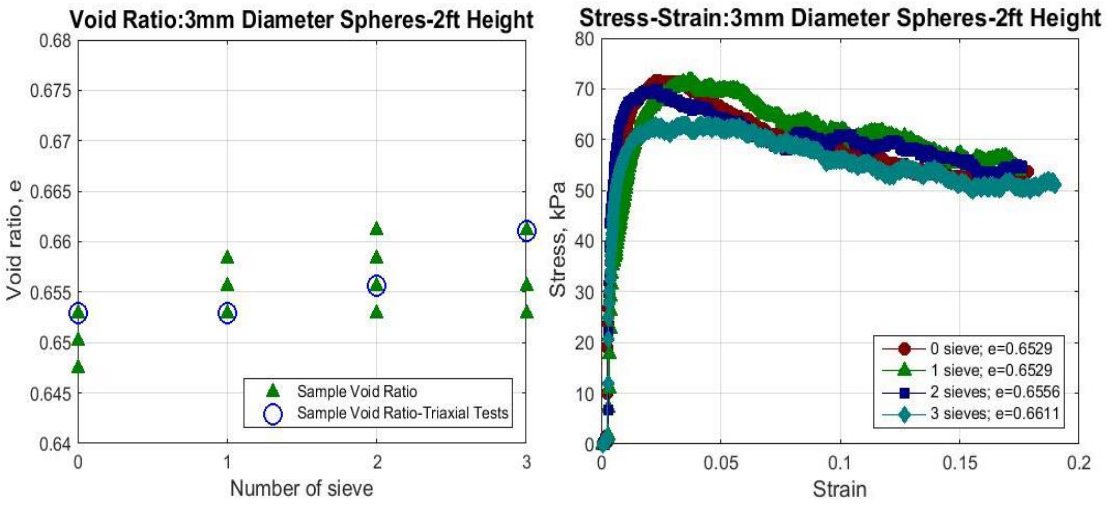

Figure 16: Stress-Strain Curves of Random 3 mm Diameter Sphere Samples Prepared at 2 ft Drop Height Subjected to Triaxial Compression.

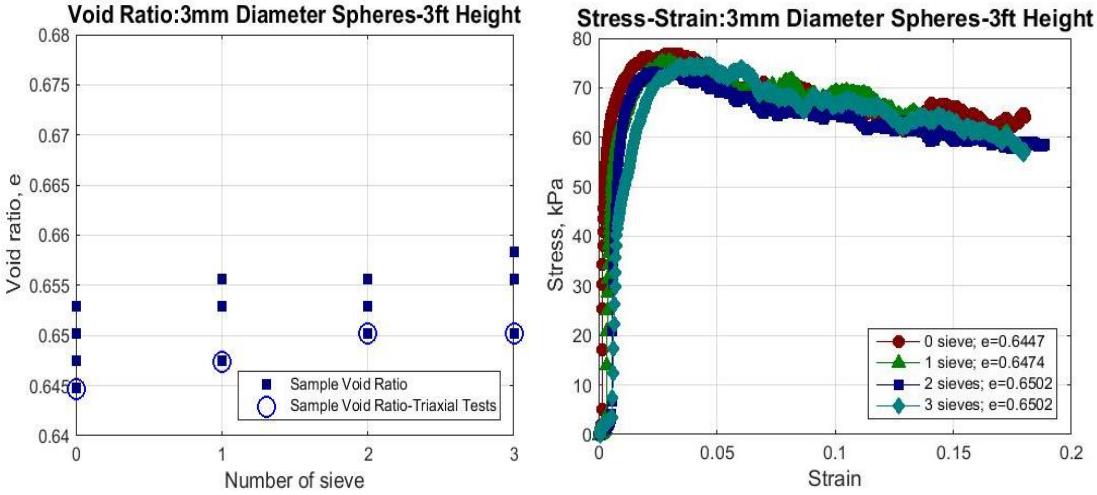

Figure 17: Stress-Strain Curves of Random 3 mm Diameter Sphere Samples Prepared at 3 ft Drop Height Subjected to Triaxial Compression.

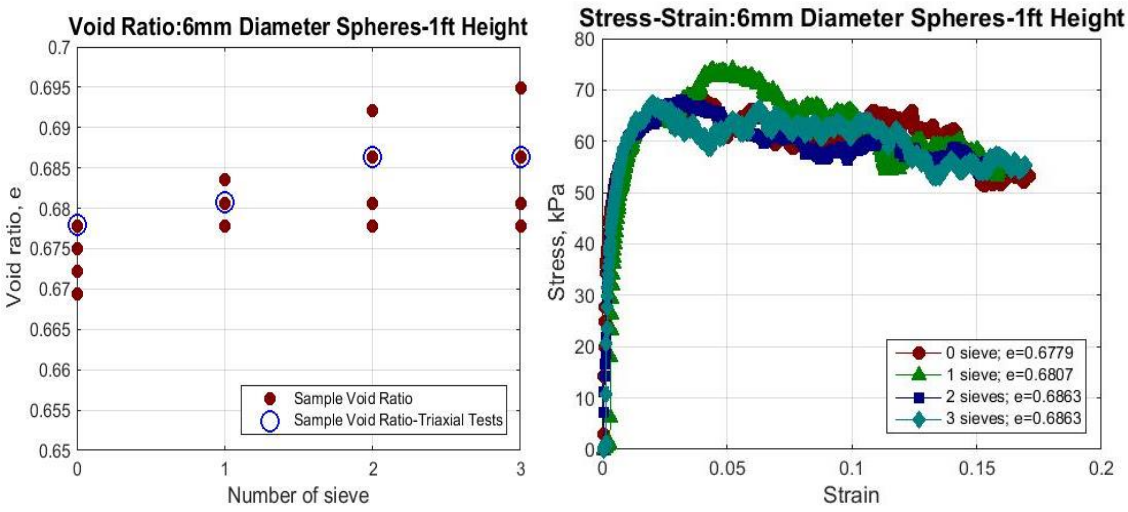

Figure 18: Stress-Strain Curves of Random 6 mm Diameter Sphere Samples Prepared at 1 ft Drop Height Subjected to Triaxial Compression.

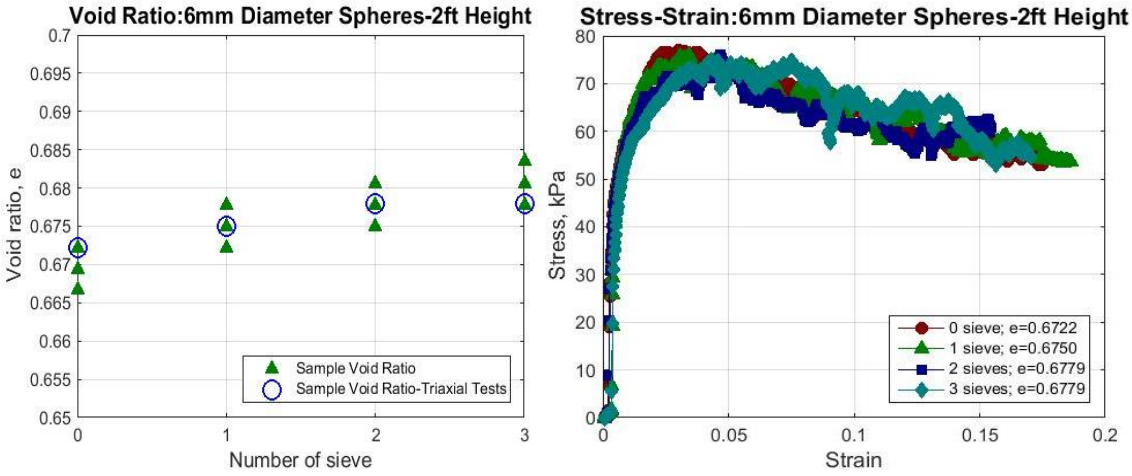

Figure 19: Stress-Strain Curves of Random 3 mm Diameter Sphere Samples Prepared at 3 ft Drop Height Subjected to Triaxial Compression.

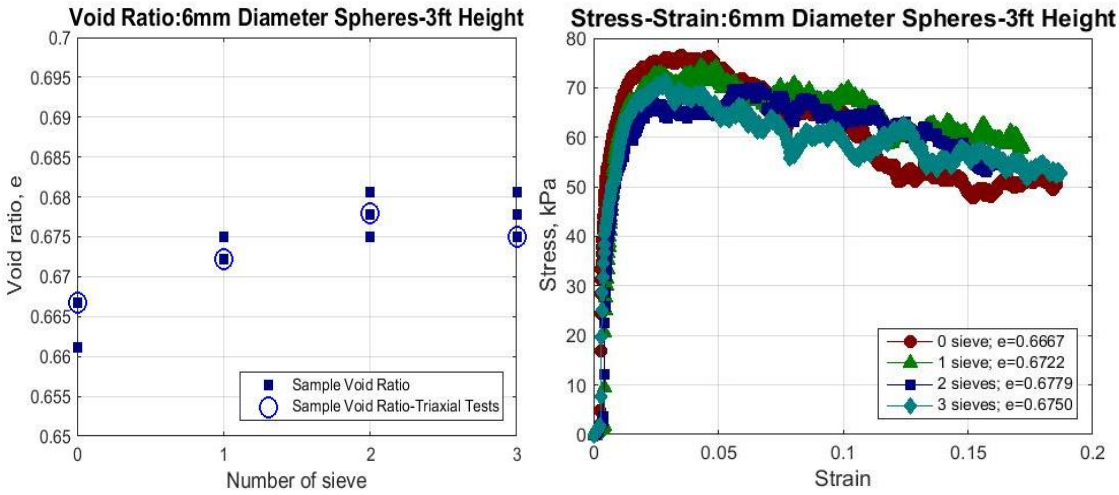

Figure 20: Stress-Strain Curves of Random 3 mm Diameter Sphere Samples Prepared at 3 ft Drop Height Subjected to Triaxial Compression.

The ultimate stress of each sample is recorded and plotted versus sample void ratio in Figure 21. It is observed that the stress strain curves indicates dense samples by having peak stresses. The ultimate stresses vary from 67 to 77 kPa for 6 mm diameter sphere samples and from 65 to 77 kPa for 3 mm diameter sphere samples. Despite the fact that void ratios of samples made of 6 mm diameter spheres are higher than void ratios of samples made of 3 mm diameter spheres, the variation of ultimate stress is almost similar. Also, samples with lower void ratio tend to reach higher peak in ultimate stress. The residual stresses are taken at 15% strain for all sample. Plots of void ratio versus residual stress are presented in Figure 22 for both 3 mm and 6 mm particle size samples. It is observed that the residual stress of samples made of 6 mm diameter spheres fluctuates from 51 to 59 kPa while the residual stress of samples made of 3 mm diameter spheres varies from 51 to 66 kPa. Notice that the correlation between void ratio, residual stress

and sample preparation conditions does not show a clear pattern as those observed in Figure 21.

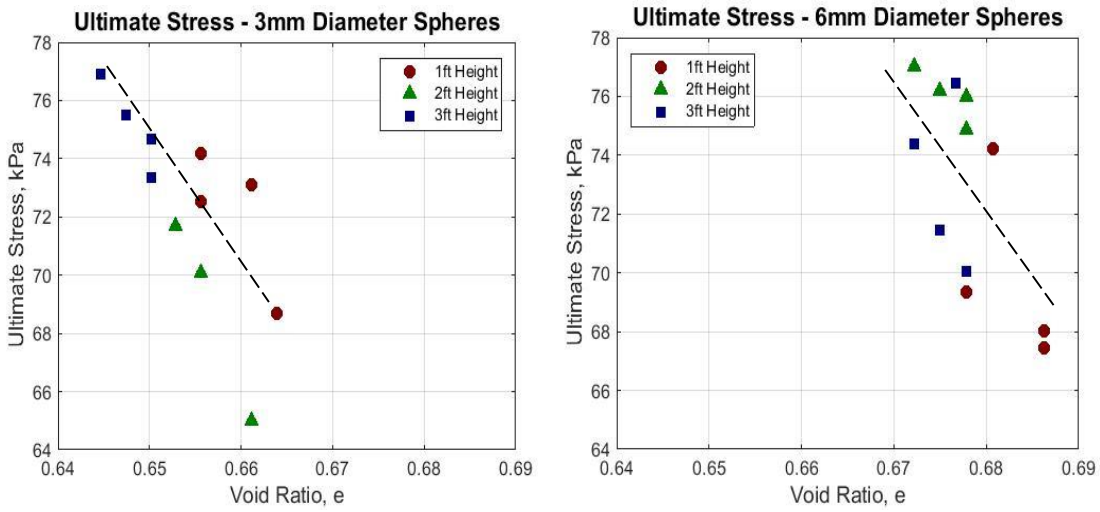

Figure 21: Ultimate Stress of 3 mm Diameter Sphere Samples (Left) and 6 mm Diameter Sphere Samples (Right) versus Void Ratio.

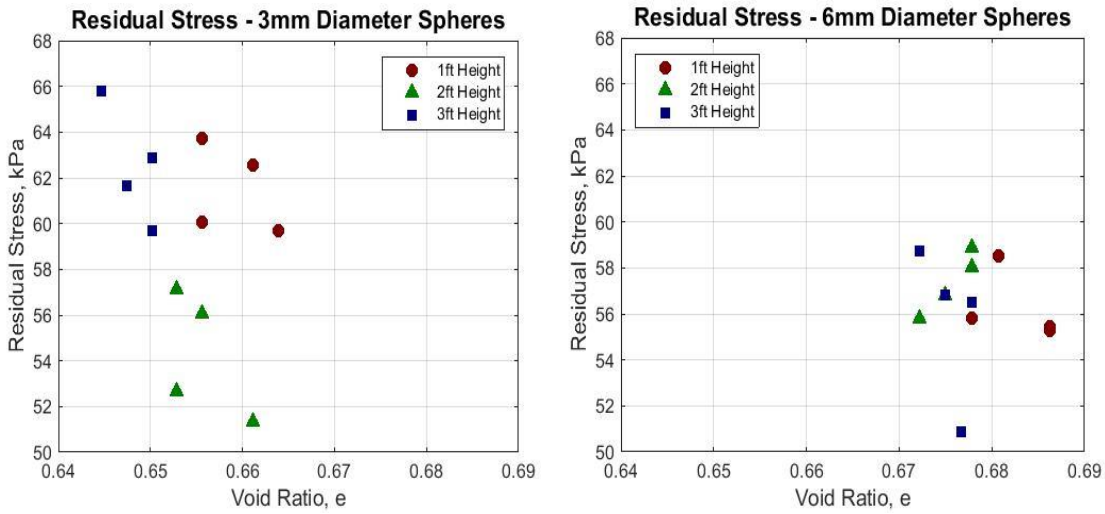

Figure 22: Residual Stress of 3 mm Diameter Sphere Sample (Left) and 6 mm Diameter Sphere Sample (Right) versus Void Ratio at 15% Strain.

CHAPTER IV

X-RAY COMPUTED TOMOGRAPHY

4.1 X-Ray Computed Tomography (CT)

X-Ray tomography is a technique based on the X-Ray diffraction analysis to retrieve the location of the particles inside the mold [25]. In this work, the purpose for performing an X-Ray tomography is to investigate the heterogeneity of the reconstituted sample to use as an initial condition in DEM analysis for the shearing of the specimen. This method provides an understanding of how the specimen is composed under different sample preparation methods and an observation of the non-uniformity of the specimen in terms of the volume of voids created during specimen preparation. At first, X-rays CT images of selected samples are taken. Then, the images are analyzed to locate the centroid positions of all particles to obtain the spatial particle configuration along the specimen height.

The CT scan images are taken at the Chevron Petrophysical Imaging Laboratory of the Petroleum Engineering Department at Texas A&M University. The samples are prepared in the Chevron lab then taken to the X-rays room for taking images to reduce the chance of disturbing the sample when moving between two labs. The mold is removed and the sample is rotated horizontally while the vacuum pump is still intact with the sample to reserve the internal structure integrity of the sample. Thus, any possible X-rays scattering during scanning can be minimized. A base made of cardboard paper is built to perfectly fit the specimen while it is placed on the bed of the X-rays scanner. CT scan images taken along the length of the specimen with interval of 1 mm. Two samples of 3

mm and 6 mm diameter spheres prepared at the condition of 0.9144 m drop height with 3 sieves. Figure 23 shows the arrangement of the sample before taking X-rays scan. The analysis of CT scan images is later performed to obtain spatial heterogeneity condition of the sample.

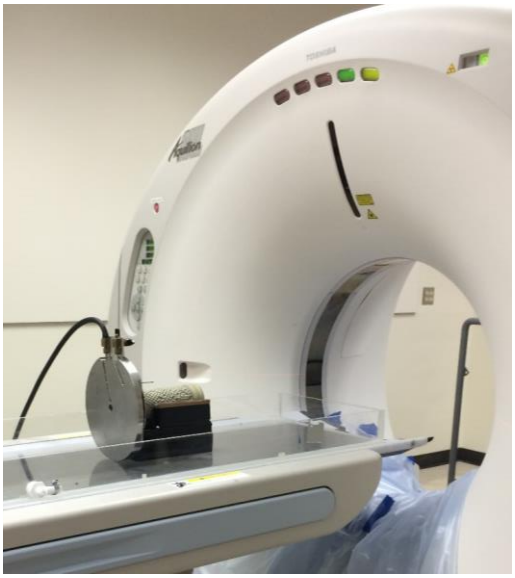

Figure 23: Setup of Specimen for X-rays CT Scans.

4.2 Digital Image Analysis

The CT scan images are processed using the image processing toolbox in MatLab [34]. At first, the image contrast is enhanced and noise is removed by 1%. After that, a histogram of the image is retrieved to obtain the gray scale distribution of the image. Based on the information from the histogram, a binary image is generated by thresholding the raw image at the grey scale intensity of 3900 to remove the cardboard base and obtain only spheres in the image. A binary scheme is applied where all pixels that below the

threshold level are set to equal zero and all other pixels are set to equal to one. Morphological closing is performed on the binary image to fill the voids inside the spheres. Then, the inverse of the closed binary image is subtracted from the original image. Figure 24 shows step by step image processing process discussed above. Since the X-rays CT scan machine is originally for medical purposes, the X-rays intensity is not customized to for metals with such high density like steel, which leads to the metal artifacts effect in the image. Due to the amount of noise in the raw image, it is impossible to reduce noise without scarifying the spheres information. Further image analysis to identify the centroid of each spheres has not been completed yet. Also, the use of other materials that are less dense than chrome steel has been considered for exploration purposes.

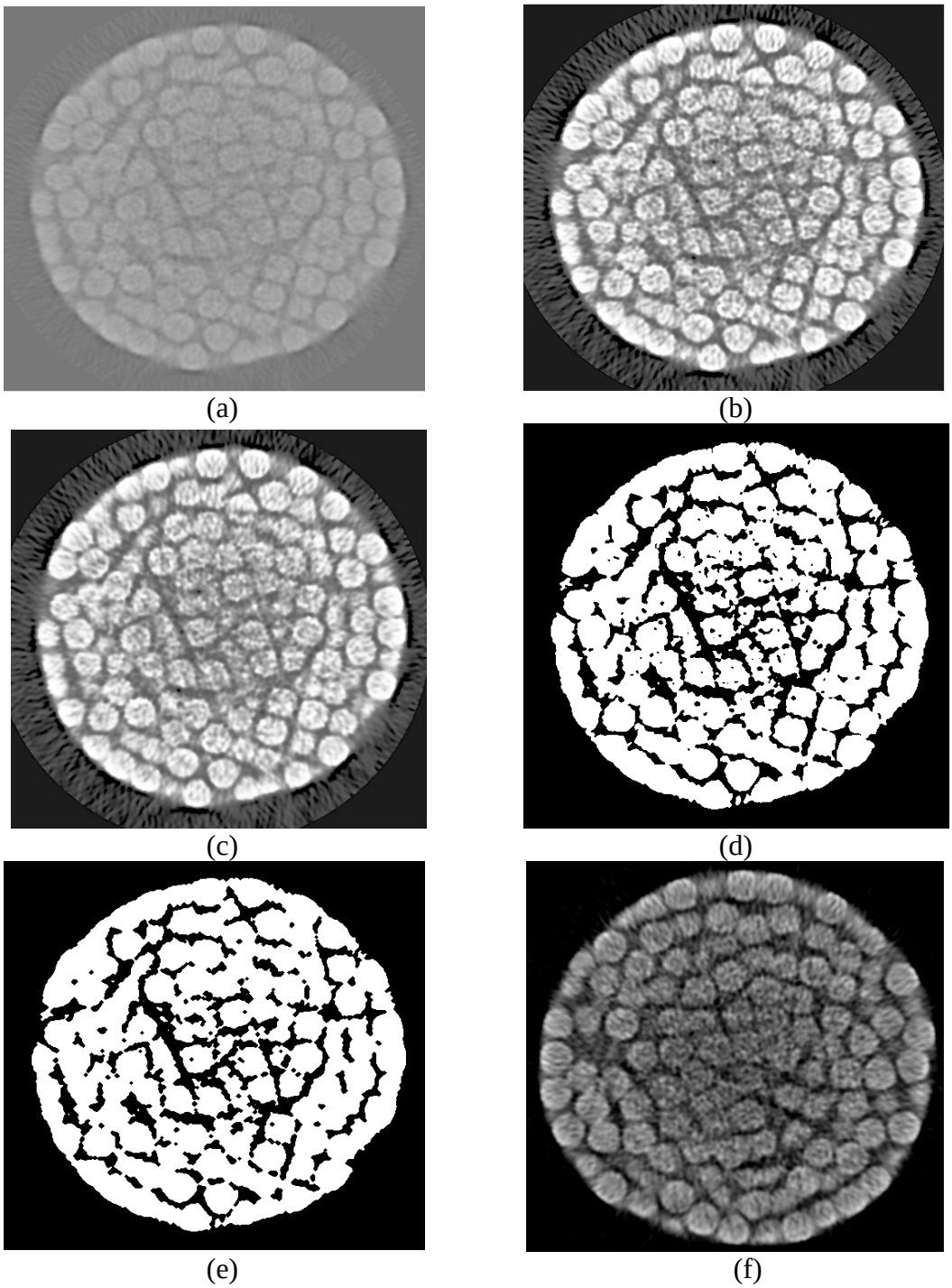

Figure 24: Image Processing of a Slice 20 mm from the Bottom of a Sample with 6 mm Diameter Spheres. (a) Original Image, (b) Contrast Enhanced, (c) Noise Reduction, (d) Binary Image, (e) Morphological Closing of Binary Image, and (f) Cross-section with Mold Removal.

CHAPTER V

DISCRETE ELEMENT MODELS

5.1 Background

The study of complex dynamic behavior of particle systems has been a crucial topic for researchers in recent decades, especially in the geotechnical field. PFC (Particle-Flow Code) was first developed by Cundall in 1971 following the Distinct-Element Method (DEM) to simulate rock-mechanics problems then applied to soils problems in 1979 [18]. PFC is classified as discrete element code since it allows distinct particles that displace and rotate independently to each other, and the particles interact only at contacts or interface between them while automatically recognizing new contacts at the end of each calculation cycle. Herein, all particles are treated as rigid bodies. PFC follows the "soft-particle" approach that allows the particles to deform by overlapping each other at the contact points. Also, multiple particle contacts can occur simultaneously and the contact duration is considered finite which are essential for modeling quasi-static systems. The particles always remain geometrically rigid during contact and the deformation is taken into account in the force models. PFC defines particle bodies as balls and clumps where balls are rigid disks (in 2D) or spheres (in 3D) and clumps are collections of rigid balls (pebbles) overlapping each other with no contact formed in between the balls. Clumps are used to simulate irregular shape particles. Another body type in PFC is wall which is a collection of facets to form a manifold and orientable surface. Motion of balls and clumps follows Newton's Law of Motion while motion of walls is specified by users.

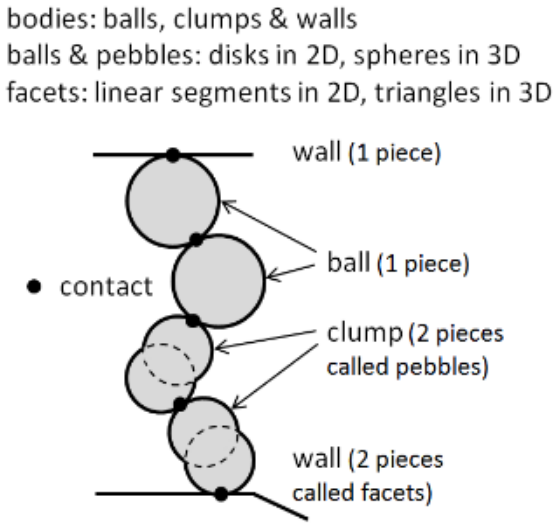

Figure 25: PFC Model Components [35].

5.2 Calculation cycle in PFC

As mentioned in the PFC3D User's Manual [35], PFC adopts a time-stepping algorithm which alternates between the force-displacement law to each contact and the Newton's Second Law (Law of Motion) to each particle and constantly updates particles positions during every calculation cycle. At the beginning of each calculation cycle, all particle positions and contact information is carried on from previous calculation cycle. Then, the force-displacement law is applied to each contact using those information to obtain contact forces based on the relative motion between two entities and the contact constitutive law models. After that, the law of motion is applied to each particle to update the particles' position and velocity based on the resultant contact forces from previous step and any external forces applied. Finally, new particle positions and surface positions are updated to be passed to the next calculation cycle.

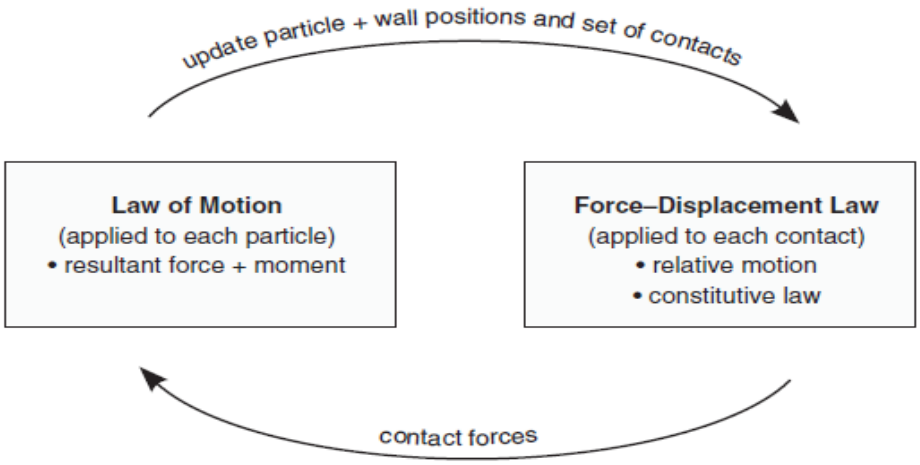

Figure 26: Calculation Cycle in PFC [36].

5.3 Contact Constitutive Models

The constitutive contact model in PFC3D includes three components: a stiffness model, a slip model and a bonding model [36]. The PFC3D manual has a full description of each models used in the program. The following description of linear-based models is summarized from the PFC3D manual. Bonding models, including linear-based models, smooth-joint contact model and flat-joint contact model which are used to replicate cohesive materials such as rocks behaviors, are not mention here.

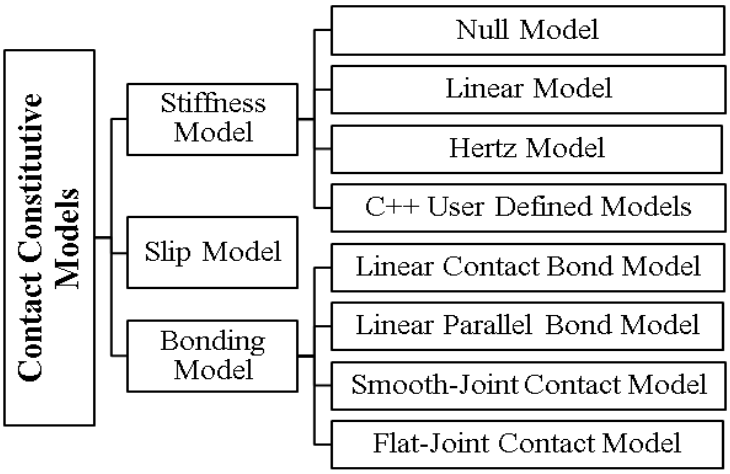

Figure 27: Contact Constitutive Models in PFC.

5.3.1 Stiffness Model

The stiffness model provides a linear relation between the contact forces and the relative displacement in the normal and shear directions. The elements of the stiffness model are normal stiffness (K^n) and shear stiffness (k^s). Normal stiffness, also named as secant stiffness, relates the total normal forces to the total normal displacement.

$$K_i^n = K^n.\ U^n.n_i$$

Shear stiffness, tangent stiffness, relates the increment of shear force to the increment of shear displacement.

$$\Delta F_i^s = -k^s\ .\Delta U_i^s$$

The stiffness model can be assigned for linearly response or nonlinearly response (Hertz model), depending on the properties of the materials. The linear stiffness model is set default in PFC.

5.3.1.1 Null Model

A null contact model preserves internal force equal to zero for newly created contact without any specification for the contact model.

$$F_c \equiv M_c \equiv 0$$

5.3.1.2 Linear Stiffness Model

Here is a brief summary of the linear stiffness model. Components of the linear contact model are shown in Figure 28.

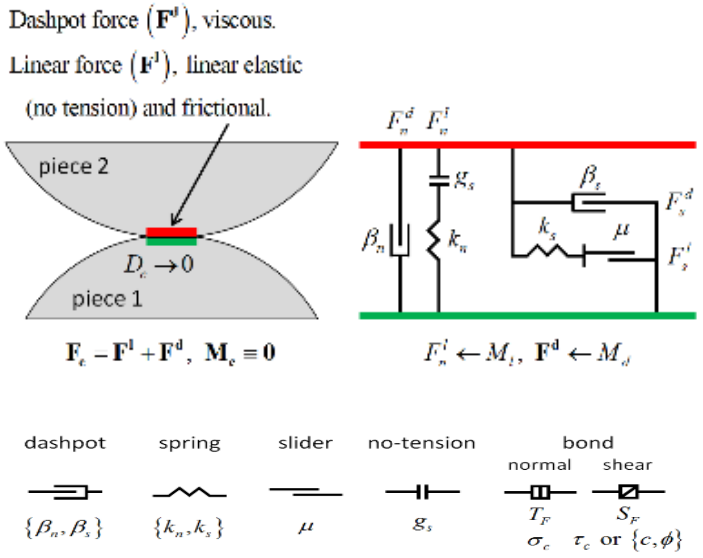

Figure 28: Rheological Components of the Linear Contact Model [35].

In the linear model, relative rotation of the particles is not resisted thus the contact moment equals to zero. The linear components provide linear elastic frictional behavior with no tension represents as the springs. The dashpots provide viscous behavior by

specifying the normal and shear critical damping ratios β_n and β_s. The linear stiffness model also provides the contact-bond behavior, which will be described in the following sections.

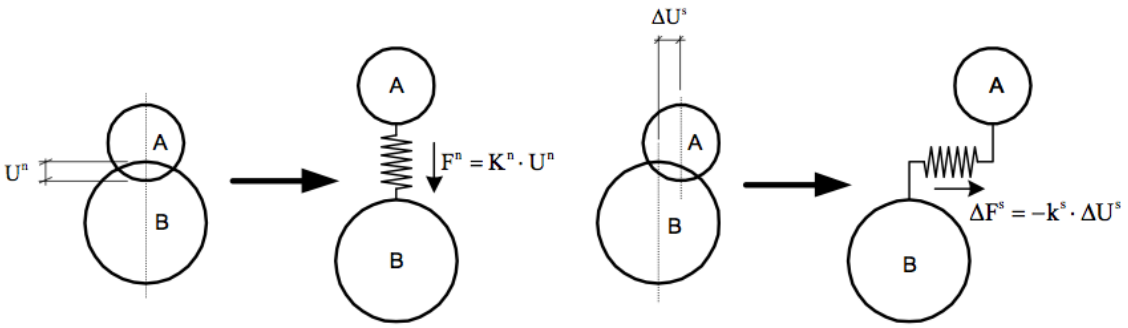

Normal Stiffness Shear Stiffness

Figure 29: Two Types of Linear Stiffness in PFC [17].

Figure 29 shows a schematic of the linear normal stiffness and linear shear stiffness between two particles. The normal stiffness (K^n) relates the normal force (F^n) to the normal displacement (U^n), so the normal stiffness can be seen as secant stiffness. The linear normal stiffness can be obtained by

$$K^n = \frac{k_n^{[A]} . k_n^{[B]}}{k_n^{[A]} + k_n^{[B]}}$$

where $k_n^{[A]}$ and $k_n^{[B]}$ are normal stiffness of particle A and B relatively.

The normal secant stiffness is also equal to the normal tangent stiffness in the linear stiffness model since

$$k^n \equiv \frac{dF^n}{dU^n} = \frac{d(K^n U^n)}{dU^n} = K^n$$

The shear stiffness (k^s) relates the increment of shear force (ΔF^s) to the increment of shear displacement (ΔU^s) so the shear stiffness can be seen as tangent stiffness. The linear shear stiffness can be calculated as listed below

$$k^s = \frac{k_s^{[A]} . k_s^{[B]}}{k_s^{[A]} + k_s^{[B]}}$$

where $k_n^{[A]}$ and $k_n^{[B]}$ are normal stiffness of particle A and B relatively.

5.3.2 Slip Model

The slip model enforces a relation between the shear and normal forces so that two contact particles may slip relatively to one another. The slip model ensures that the shear force component (F^s) always remain less than the product of normal force component (F^n) and friction coefficient (μ). The slip model is represent as sliders in the schematic presentation of contact models. The equation for slip model is shown below

$$F_{max}^s = \mu \, |F_i^n|$$

If the normal force exceeds the maximum shear force then slip will occur in the next calculation cycle by the equation $F_i^s \leftarrow F_i^s \, (\frac{F_{max}^s}{|F_i^s|})$

5.4 Model Parameters

A question arises that which contact model should be used in this study. Since the steel spheres are discrete and not glued together, bonding models are disregarded. The linear contact model is selected based on previous study done by Noble [25]. Macro-parameters for PFC model are similar to material dimensions and material properties used in the

sample preparation experiments, including wall dimensions, ball diameter, ball density; friction coefficient of ball and ball, wall and ball. By doing this, a probabilistic down scaling procedure to map from macro-parameters to micro-parameters can be introduced. A list of model parameters is presented on Table 4.

Table 4: Ball Input Parameters in DEM Model

DEM parameters	Unit	
Ball diameter	mm	3; 6
Ball density	kg/m^3	$7.8x10^3$
Ball shear modulus	Pa	$7.9x10^{10}$
Ball-ball friction coefficient	-	0.096
Ball-wall friction coefficient	-	0.28
Ball normal stiffness	Pa	$2.01x10^{11}$
Ball shear stiffness	Pa	$7.9x10^{10}$

5.5 Sample Formation Procedure - Radius Expansion

PFC support document provide a method to generate homogeneous specimen with specific non-zero material pressure [36]. This procedure includes a packing phase, which creates a grain assembly, and a finalization phase, which assigns contact properties and additional material properties that will be assigned to future contacts. At first, random particles are based on specified porosity. Then, friction coefficient between particles is set to zero for the particles to rearrange until the mean stress near zero or achieve static-equilibrium condition. During this step, most of the overlaps are eliminated to prepare for the next step. Particle size is modified until the mean stress is within the pressure tolerance of the defined sample pressure and static-equilibrium condition has been achieved. In the

finalized phase, final material properties are assigned to contacts and additional material properties are specified for future material contacts. In this sample preparation procedure, specimen pressure is set equal to the confining pressure in the experiment of 55 kPa, similarly to the actual triaxial test confining pressure, and the initial porosity is equal to the global porosity value obtained from the sample preparation. Pressure tolerance ratio is set equal to 0.1. Also, the expansion factors for both the mold and the balls are set equal to one, meaning that the dimension of the particles and the mold are unchanged. Other material properties are introduced in section 5.4, such as wall dimensions, ball diameter, ball density; friction coefficient of ball and ball, wall and ball. Figure 30 shows the sample generated following the support document.

Figure 30: DEM Sample Generated by Radius Expansion Method.

5.6 Sample Formation Procedure - Air Pluviation Method

The goal is to achieve similar specimen densities for the same experimental sample preparation method as well as using such model from sample preparation to simulate a

standardized compression test. This method for simulating compression test is different from ITASCA's proposed method in the manual where the sample is prepared using the radius expansion method to achieve a desired sample porosity. Generally, multiple walls are created and welded together to form the shape of a mold, a tube and a funnel. The sieve is made of cylinder walls of 1 mm diameter replicating the configuration of the meshes. The linear contact model is used in the air pluviation model. Only gravitational force is activated as an external force applied on the sample throughout the process. At first, balls are generated above the funnel, a wall is created to cover the discharge opening of the funnel. Then one million cycles are run to have the spheres deposited inside the funnel and come to rest. After that, the wall at the end of the funnel is deleted to release all the ball. About 25 million cycles are run to have all the balls constituted into the mold. Due to time limitation, only 6 samples made of 6 mm diameter spheres are simulated for the following conditions: 0.3048 m drop height-1sieve, 0.6096 m drop height- 1sieve, 0.9144 m drop height- 0, 1, 2, and 3 sieves. Figure 31 presents PFC model replicating sample preparation process using air pluviation method.

Figure 31: DEM Sample Generated by Air Pluviation Method.

The velocity of the spheres are investigated as they fall out from the funnel in to the tube to compare with the spheres velocity from actual experimental results. The spheres velocity increases as they free fall from the funnel end due to constant acceleration. The spheres velocity is also affected by number of sieves placed on top of the acrylic tube. The velocity of the spheres of the samples with 0 sieve and 3 sieves on the fall tube are shown in Figure 32 and 33. Only the velocity of spheres within the first 0.15 m of the tube is considered to compare with the spheres velocity obtained from Tracker program. For the case of no sieve on the acrylic tube, the velocity increases from 1.5 to 2.5 m/s within 0.15 m into the tube. For the case of 3 sieves installed, the initial spheres velocity as they enter the tube reduces because the energy is dissipated by contacting with the sieves. The velocity varies from 1 to 2 m/s for the first 0.15 m in the tube. The range in spheres velocity in the PFC model is about the same with the spheres velocity obtain from the Tracker

analysis. From this result, it can be concluded that the spheres velocity is consistent between the experiments and simulation results.

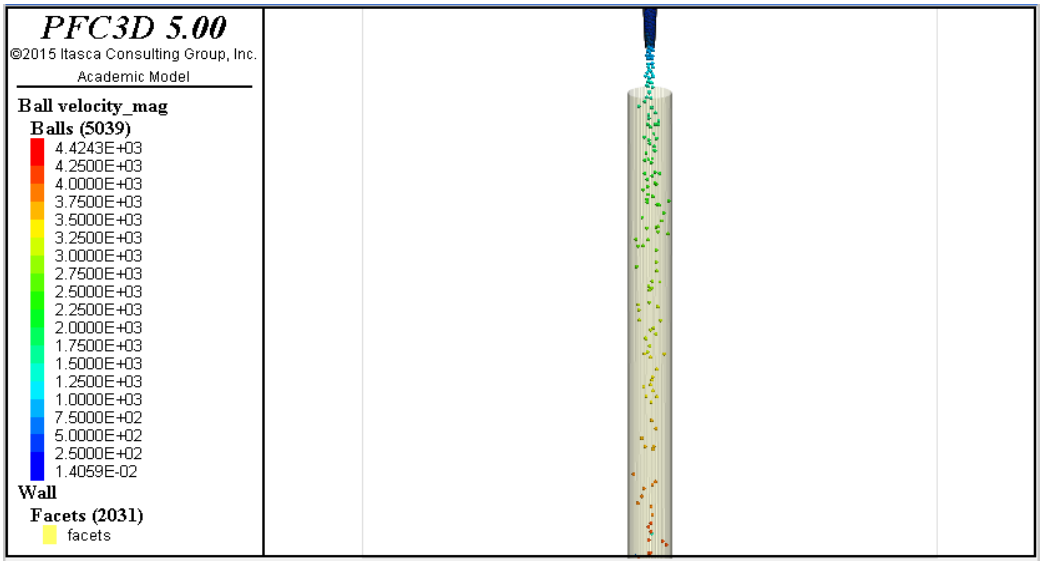

Figure 32: PFC Spheres Velocity during Air Pluviation Process for Sample Preparation Condition of 0 Sieve

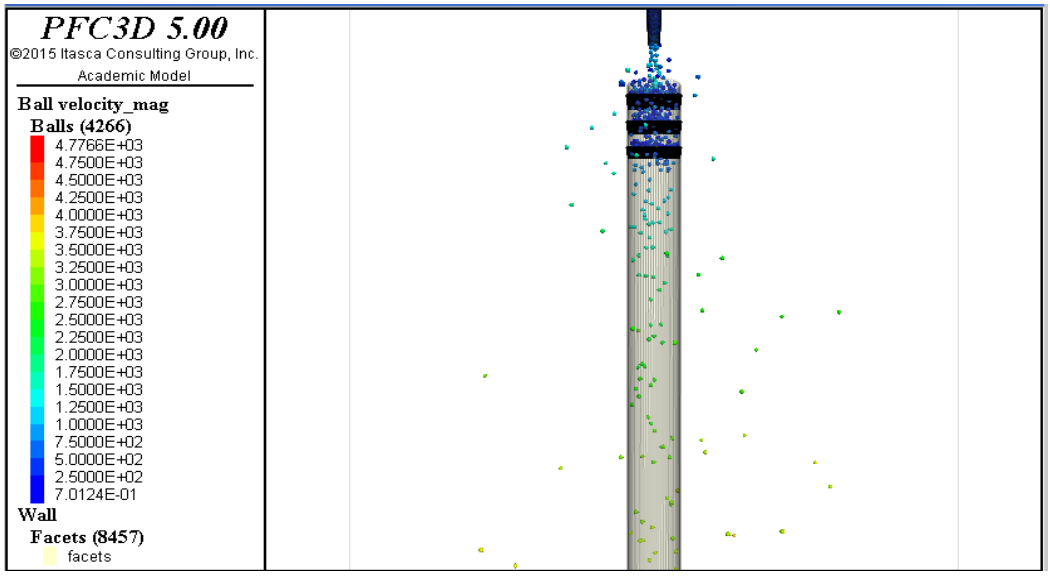

Figure 33: PFC Spheres Velocity during Air Pluviation Process for Sample Preparation Condition of 3 Sieves

5.7 Triaxial Compression Simulation

Several laboratory tests are discussed in the PFC support package including compression, diametral compression, direct tension and fracture toughness tests [36].

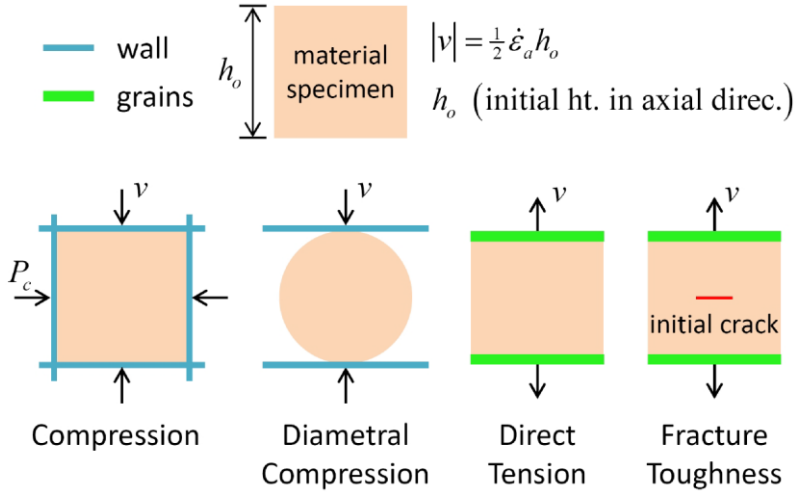

Figure 34: Laboratory Tests Supported by PFC [36].

Only compression test procedure is discussed here. During the test, the specimen is loaded by moving the axial walls whose velocities are maintained by a servomechanism to preserve constant confining pressure of within the specimen for every calculation cycle throughout the test. A pressure boundary condition activates the servomechanism to control the velocity of the top and bottom walls so that the specimen pressure is within the assigned pressure tolerance of the target pressure. The loading rate is recommended to be equal to the strain rate of the sample. Using the equation provided in Figure 34, the experiment loading rate equals to 0.0041, which would take significant computational effort. Thus, the loading rate is set 25 times faster than the recommended loading rate,

which is 0.1. A pressure boundary condition of 55 kPa that replicates the experimental confining pressure is applied to the sample. The specimen is compressed until reaches 15% strain. The compression test consists of seating phase and loading phase. The seating phase activates the servomechanism to apply a confining pressure in all directions and completes as the sample reaches the static equilibrium condition. The loading phase resets all strains to zero and then apply an axial strain to the axial walls with specified loading rate while maintaining constant confining pressure.

Due to limited time, only three compression tests are performed for samples prepared by radius expansion method. The samples subjected to the compression are prepared with initial void ratio are equal to the experimental void ratio of samples constituted from 0.9144 m drop height with 0, 1, 2 and 3 sieves. Stress-strain plots of PFC models and experimental results are presented in Figure 35 to 38.

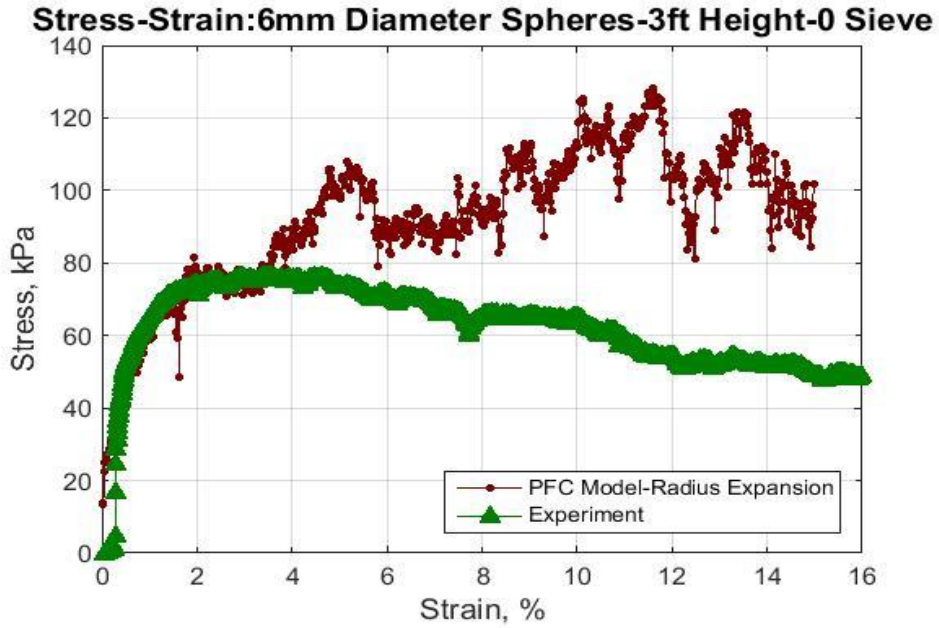

Figure 35: Stress-Strain Comparison between Experiment and PFC Simulation for Sample Preparation Condition of 3 ft Drop Height and 0 Sieve.

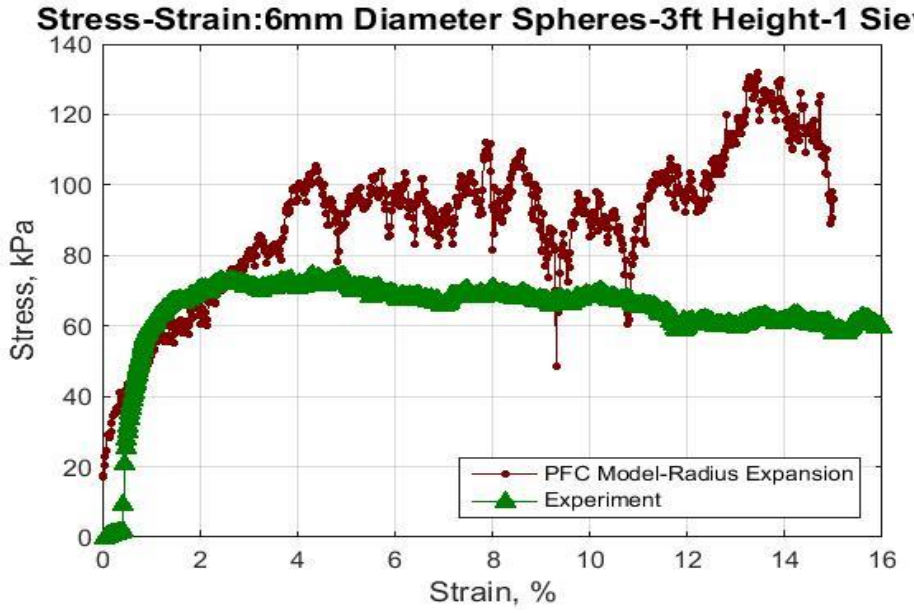

Figure 36: Stress-Strain Comparison between Experiment and PFC Simulation for Sample Preparation Condition of 3 ft Drop Height and 1 Sieve.

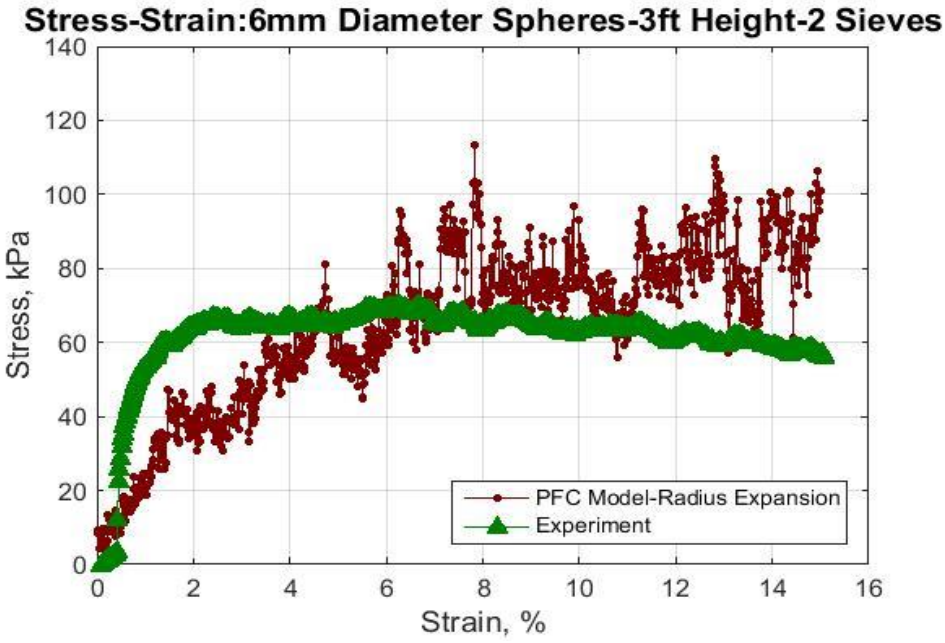

Figure 37: Stress-Strain Comparison between Experiment and PFC Simulation for Sample Preparation Condition of 3 ft Drop Height and 2 Sieves.

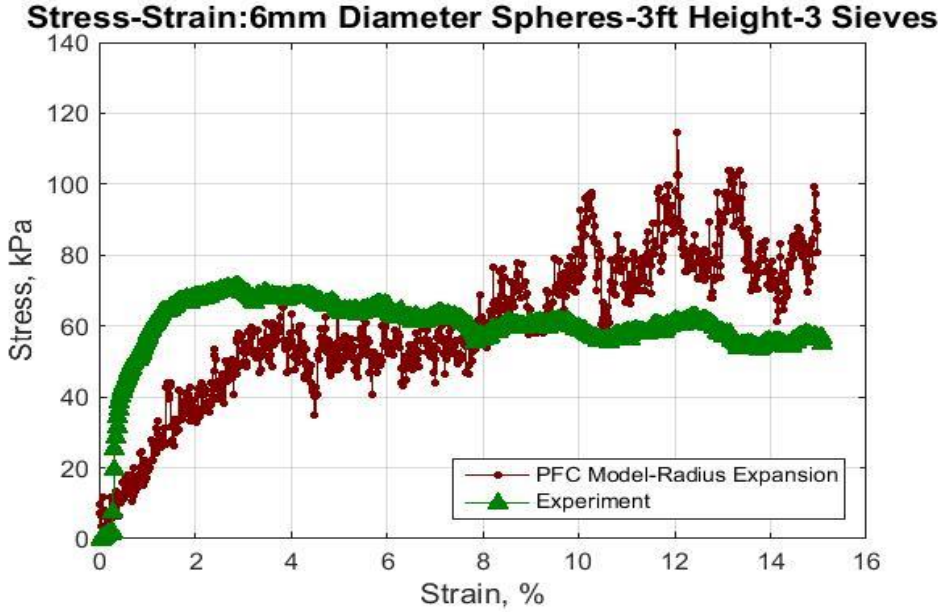

Figure 38: Stress-Strain Comparison between Experiment and PFC Simulation for Sample Preparation Condition of 3 ft Drop Height and 3 Sieves.

It is observed that the stress paths increase until it reaches the peak then slowly decreases until obtaining residual stress condition in the experiment. On the other hand, the simulation the stress path increases with high fluctuation after 8% strain. The experiment results have steeper slopes in the initial loading comparing to PFC models for samples conditioned at 0.9144 m drop height and 2 to 3 sieves. For the case of no sieve on the tube, both stress paths match the trend until reach 3% strain then differentia. Possible cause of the difference in the stress-strain responses might be setting the model loading rate incorrectly.

5.8 Computational Time

All of the PFC simulation are run in a Window server built on a super computer whose processor is the Intel Xeon E5-2695 v3 2.3 GHz chipset that has 14 cores and 28 threads. The installed memory (RAM) is 128 GB. PFC3D version 5.0 license allows running 2 instant of PFC at the same time. The configuration of the Window server is recommended by ITASCA personnel for running complex PFC models.

It is known that computational time is an important criteria to justify if the numerical models are efficient in replicating material behaviors. For sample formation in PFC, samples prepared by radius expansion method take a hundred thousand cycles, approximately 10 minutes, to complete while samples prepared by air pluviation method take 30 million cycles, approximately 3 days, to complete. The difference due to the fact that air pluviation method simulates actual physical stage of each sphere with time thus would consume more calculation cycles. The calculation time of radius expansion method can be increased or decreased by changing the pressure tolerance. For the compression test, it takes 15 million cycles or about 2 days to compress a prepared sample to 15% strain with strain rate of 0.1 and pressure tolerance ratio of 0.1. The calculation time for compression test depends on strain rate, pressure tolerance and how far the sample is compressed. To improve the computational efficiency, a parametric study should be performed to investigate the effect of each factor to the computational time of the model.

CHAPTER VI

VOID RATIO ANALYSIS

With the purpose of this study is to explore the heterogeneity of the reconstituted samples, obtaining the spatial void ratio variation is a way to investigate the heterogeneity condition of the samples. This chapter introduces different methods to measure the void ratio of the samples, including the method using measurement spheres built-in in PFC, planar void ratio analysis, and regional void ratio variation of a plane.

6.1 PFC Measurement Sphere Method

PFC has built-in feature to measure internal stress, strain, and porosity of the sample. Firstly, measurement regions (disks for 2D and spheres for 3D) are created with specify position and radius. Then the measurement spheres are specified to measure porosity within the measurement spheres. Three measurement spheres are created along the sample height whose radiuses are equal to the mold radius. Porosity is the ratio of the volume of void over the total volume. Measured porosities are averaged and converted to void ratio using the equation below:

$$e = \frac{n}{1-n}$$

where e is void ratio and n is the porosity of the sample.

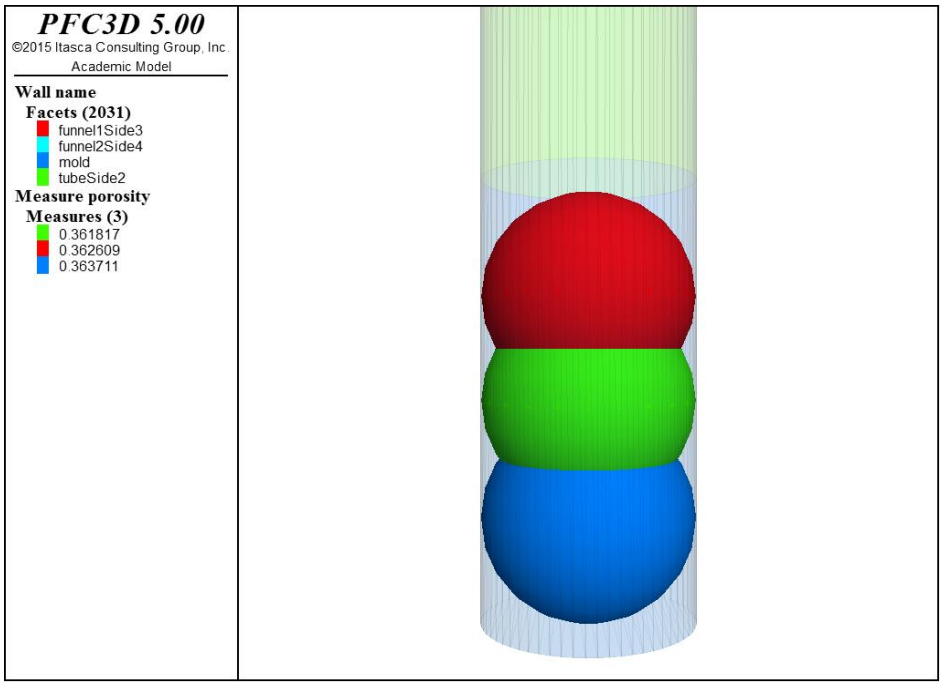

Figure 39: PFC Measurement Spheres

6.2 Planar Void Ratio Variation Method

Planar void ratio variation of the DEM model is obtained to determine if the model has capture the spatial heterogeneity of the sample. The end results provide a configuration of series of the mean planar void ratios along the sample height to compare with the global void ratio obtained from the experiment and with other methods. Centroid location of each ball is retrieved and imported into MATLAB to analyze. Distance between the center of the each ball above the sample base and certain slice height is calculated if the ball is within 3 millimeter above and below the slice height. Since the ball is perfectly spherical, the cross section of the ball is the same if the slice is above or below the ball centroid. The radius of cross section of the ball is then calculated using the Pythagorean Theorem:

$$r = \sqrt{R^2 - z^2}$$

where r is the cross sectional radius, R is the radius of the ball, and z is the distance between the ball centroid location and the slice height. Figure 40 shows the planar void ratio variation of DEM model replicating the air pluviation process from 3-foot height with 3 sieves at 20 mm from the bottom.

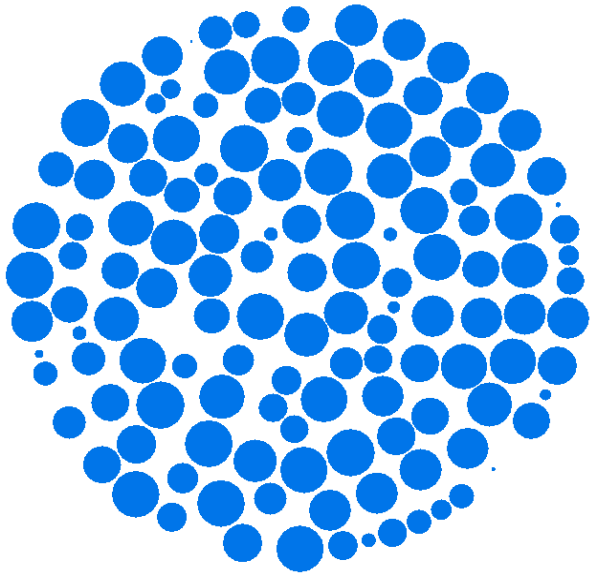

Figure 40: PFC Sample Cross Section Area of Sample at 20 mm from the Bottom, Prepared Using Air Pluviation Method at the Condition of 3 ft Drop Height and 3 Sieves

Plots of void ratio variation of PFC simulated samples using measurement spheres method and planar void ratio analysis method are presented below. The distribution of the void ratio greatly varies at near the base of the sample due to a tight packing of the balls at the sample base. Moving up the height of the sample, the variation of the void ratio deceases. At the top, the void ratio dramatically increases since there are fewer balls to fill the void.

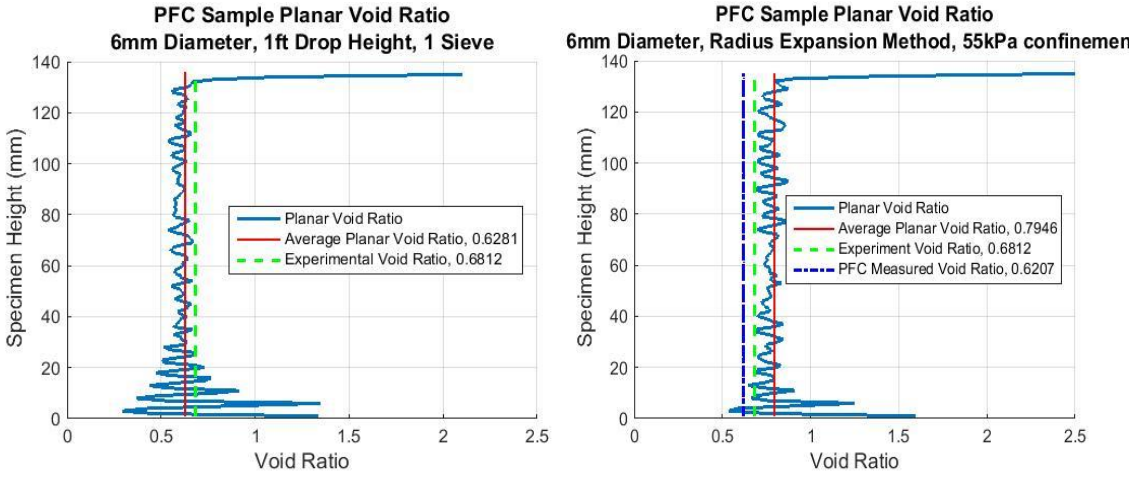

Figure 41: Comparison of Void Ratio Variation of Samples Prepared from 1 ft with 1 Sieve Using Air Pluviation Method and Radius Expansion Method

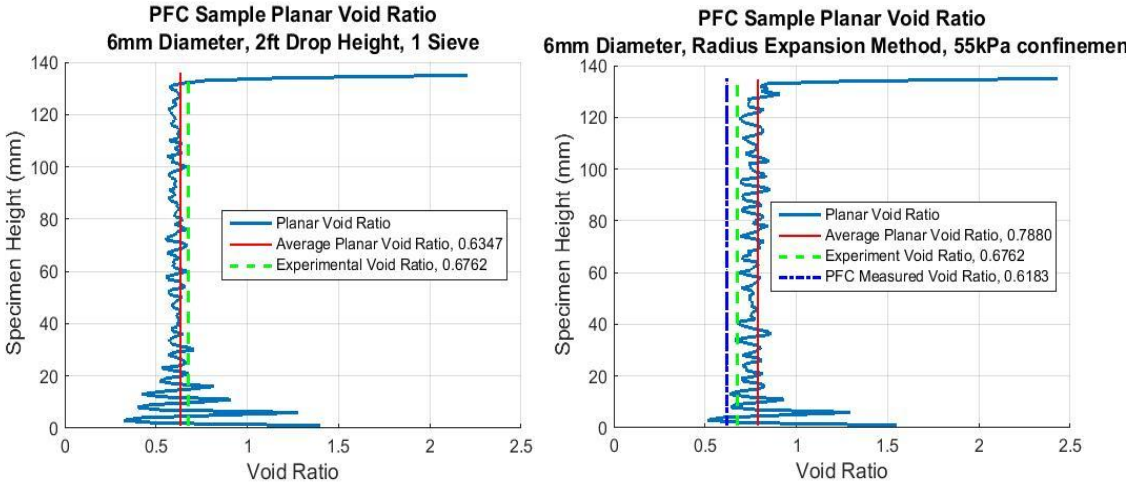

Figure 42: Comparison of Void Ratio Variation of Samples Prepared from 2 ft with 1 Sieve Using Air Pluviation Method and Radius Expansion Method

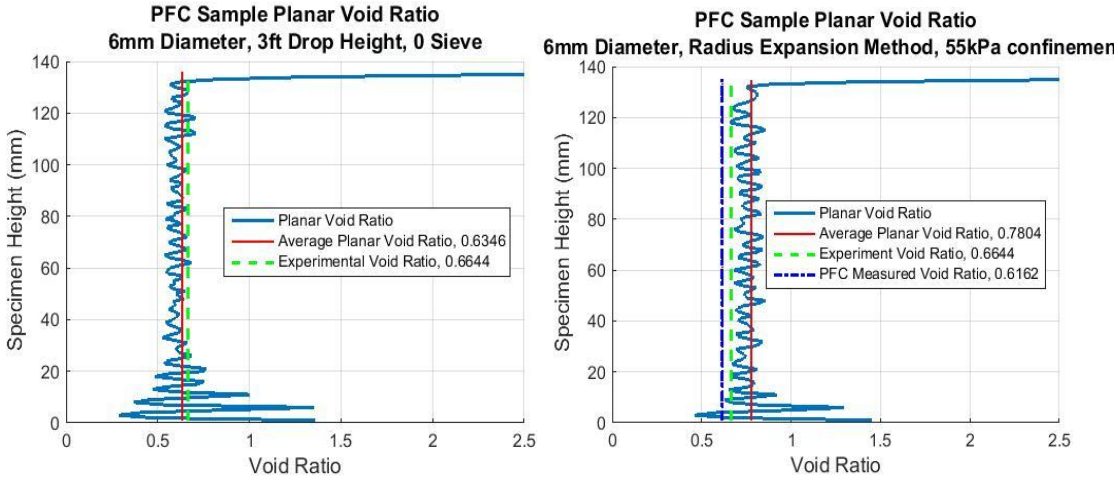

Figure 43: Comparison of Void Ratio Variation of Samples Prepared from 3 ft with 0 Sieve Using Air Pluviation Method and Radius Expansion Method

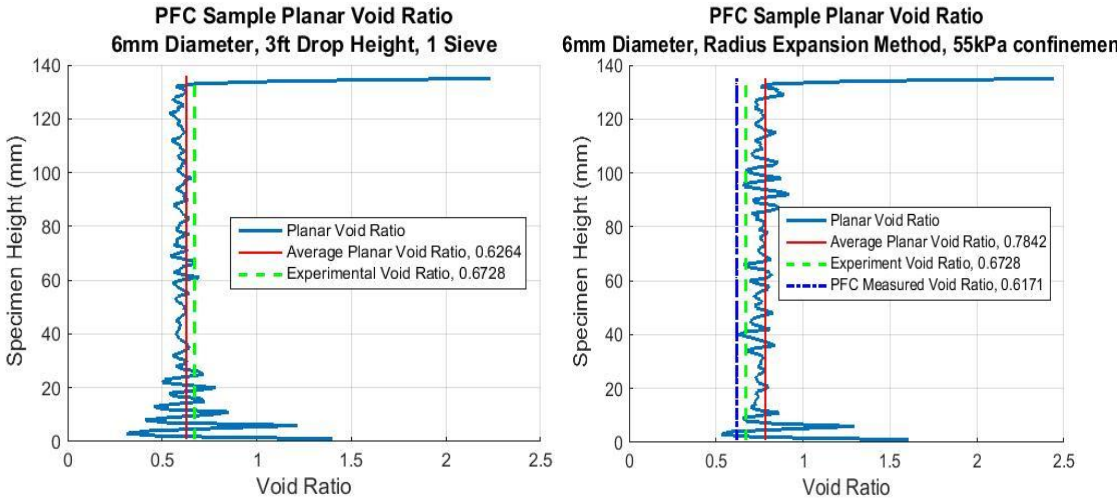

Figure 44: Comparison of Void Ratio Variation of Samples Prepared from 3 ft with 1 Sieve Using Air Pluviation Method and Radius Expansion Method

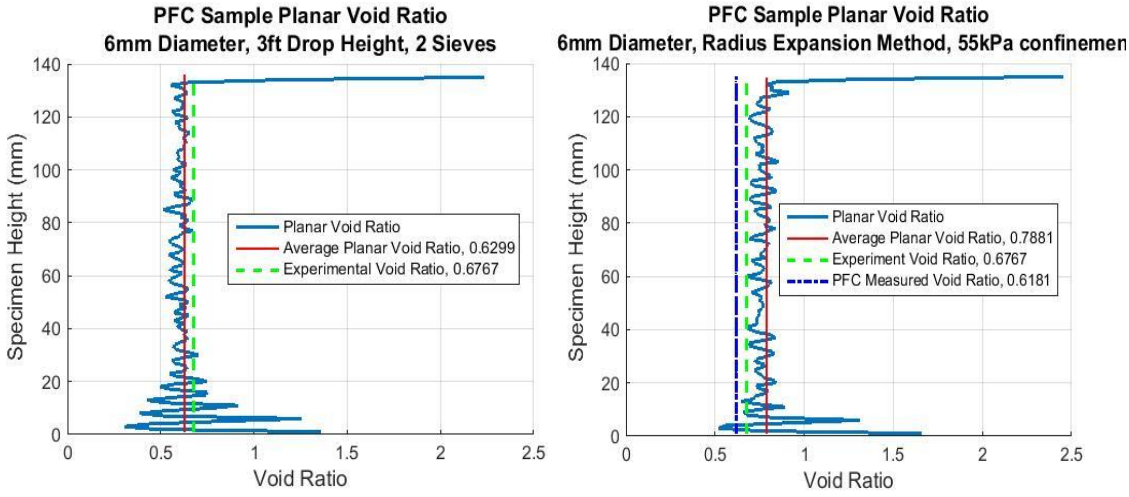

Figure 45: Comparison of Void Ratio Variation of Samples Prepared from 3 ft with 2 Sieve Using Air Pluviation Method and Radius Expansion Method

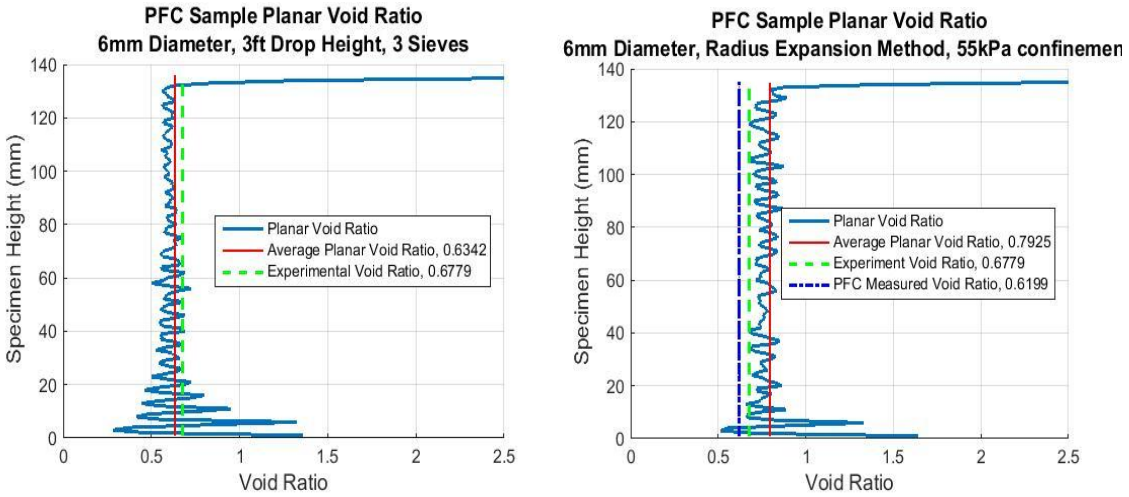

Figure 46: Comparison of Void Ratio Variation of Samples Prepared from 3 ft with 3 Sieves Using Air Pluviation Method and Radius Expansion Method

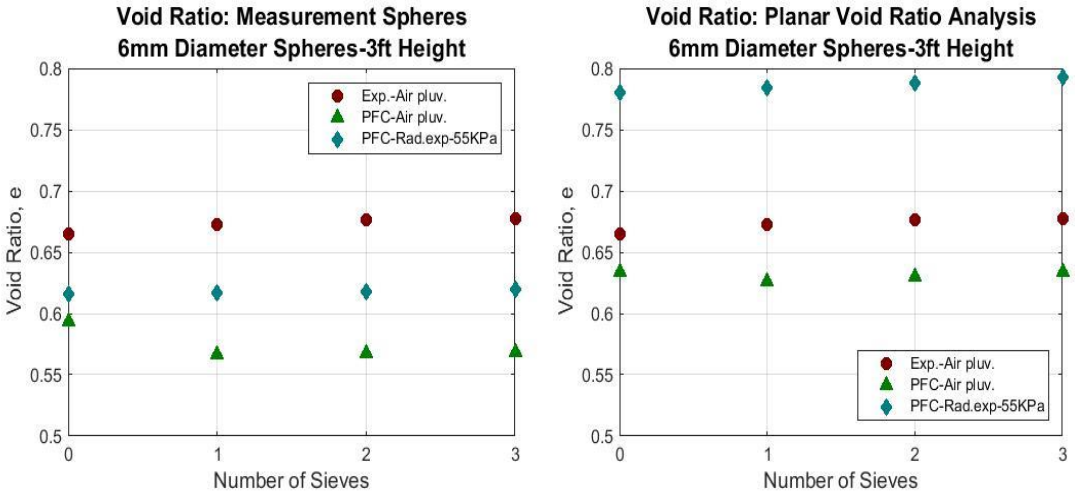

Figure 47: Void Ratio Measured using PFC Measurement Spheres and Planar Void Ratio Analysis

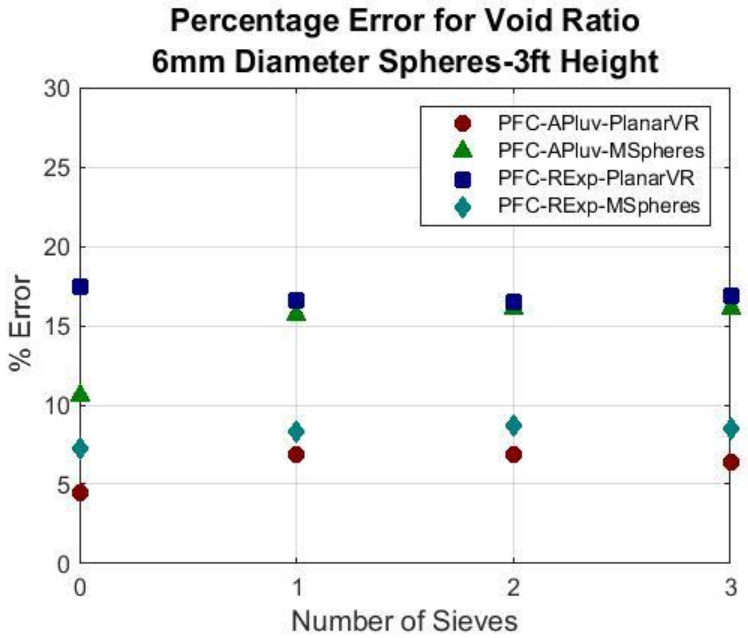

Figure 48: Percentage Error of Different Void Ratio Measurement Methods

6.3 Regional Void Ratio Variation of a Plane

Another method to examine the spatial heterogeneity of each sample is to qualify the regional void ratio variation within each plane. The void ratio variability is determined my calculated the void ratio of every control area that are equally distributed to cover the sample cross section area. At first, a multiple factor is specified to determine how many mesh circles to create whose radius change from the product of mold radius and one over multiple factor to the product of mold radius and the different between one and one over multiple factor. Then, center of the control areas are determined in a way that the arc length between every two centers is equal to each other and the distance between two mesh circles is equal to each other as well. The multiple factor is decided to be 9 so that the radius of the control area equals 1/9 of the mold radius, and equals 28 pixels. The location of the control points can be seen in the plots below. This method of creating radial mesh within the cross section guarantees maximum coverage of the control areas on the cross section. Figuer 49 shows the cross section area of the sample covered by the controls areas. After that, void ratio of each control area of equal radius are calculated. Contour plots of cross section areas at 10 mm, 40 mm, 80 mm, and 120 mm from the bottom of the models replicating samples prepared at 3 ft drop height with 3 sieves are shown in Figure 50 to 57 along with plots of the control areas within the sample cross section. The contour plots are generated by first create a meshgird of x and y directions, then interpolate the void ratio corresponding to the control area center positions in both x and y directions using ‘griddata’ command into the meshgrid.

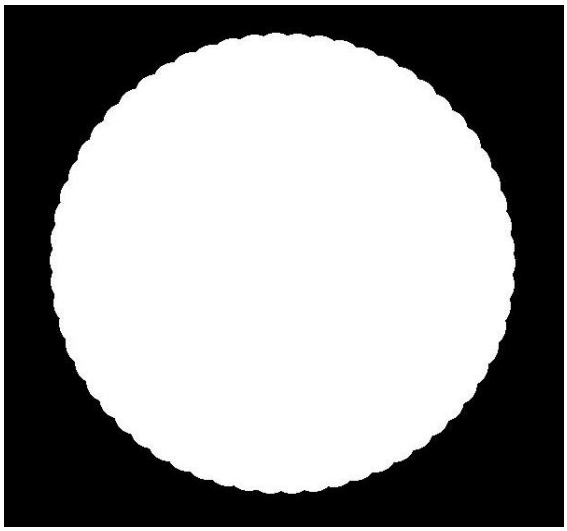

Figure 49: Specimen Area Covered by Control Areas

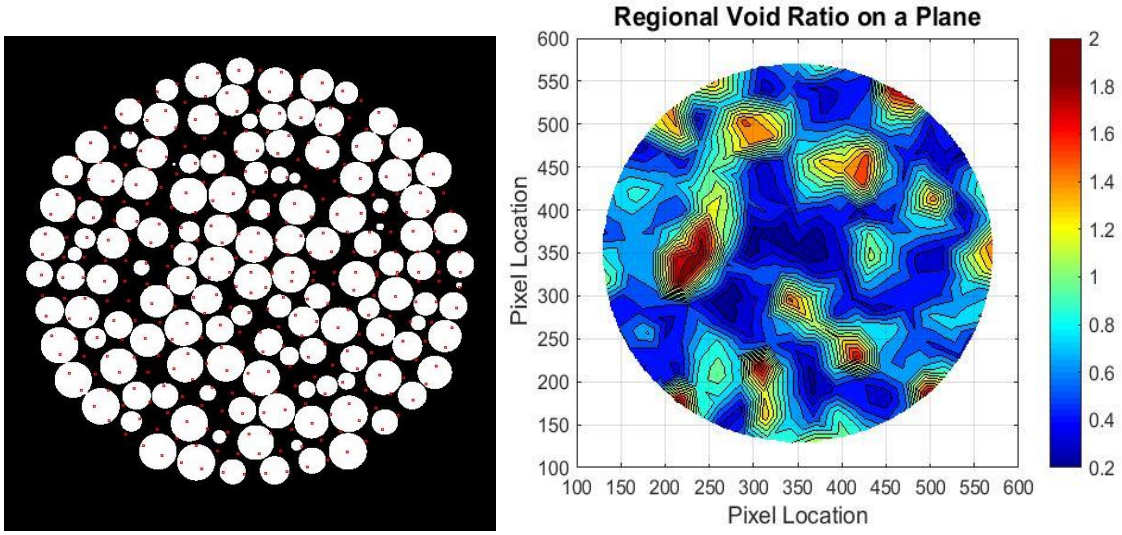

Figure 50: Center of Control Areas (Left) and Regional Void Ratio Variation (Right) at 10 mm from the Bottom of Sample Created by Radius Expansion Method

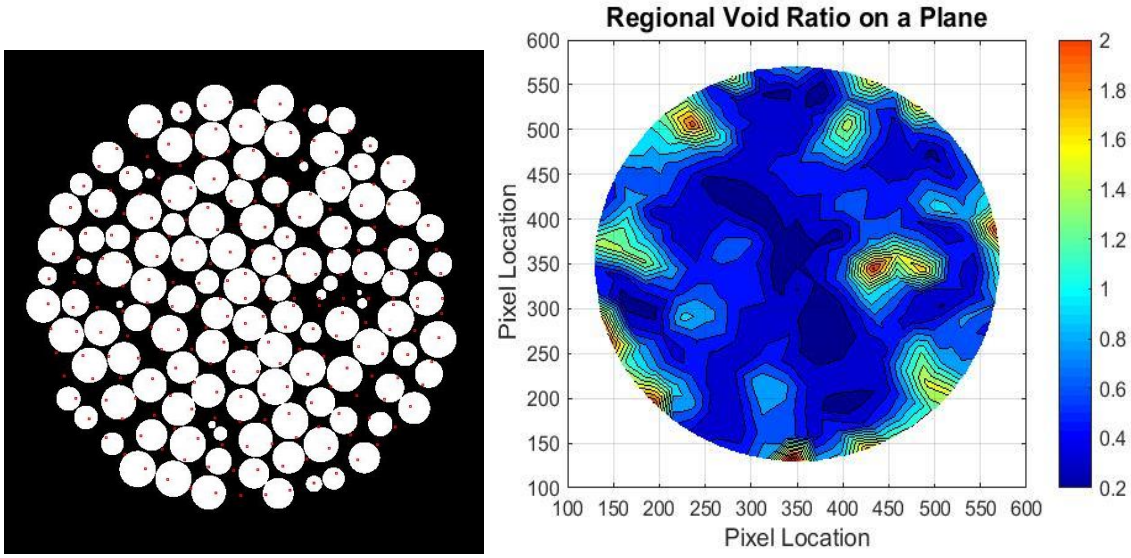

Figure 51: Center of Control Areas (Left) and Regional Void Ratio Variation (Right) at 40 mm from the Bottom of Sample Created by Radius Expansion Method

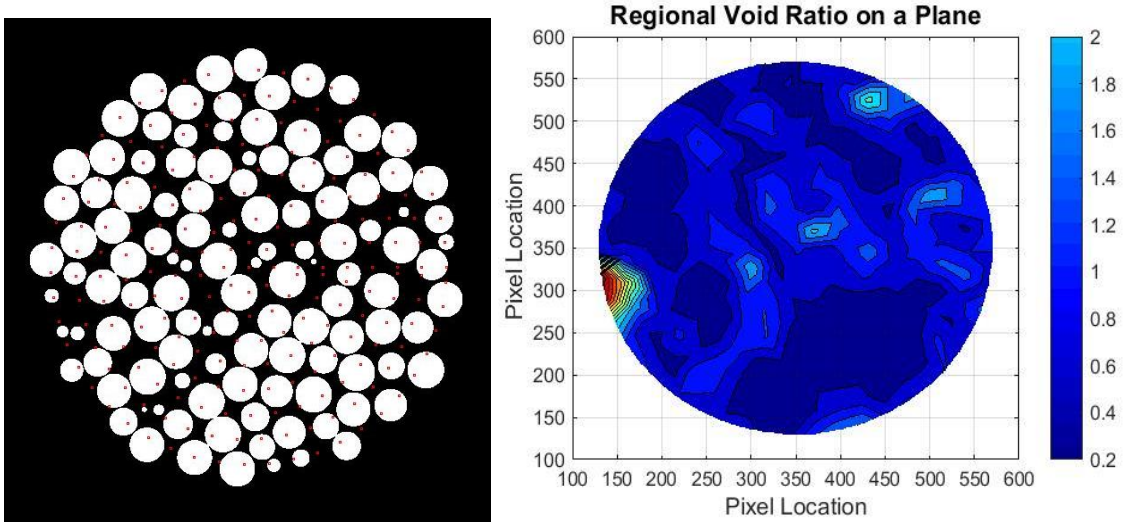

Figure 52: Center of Control Areas (Left) and Regional Void Ratio Variation (Right) at 80 mm from the Bottom of Sample Created by Radius Expansion Method

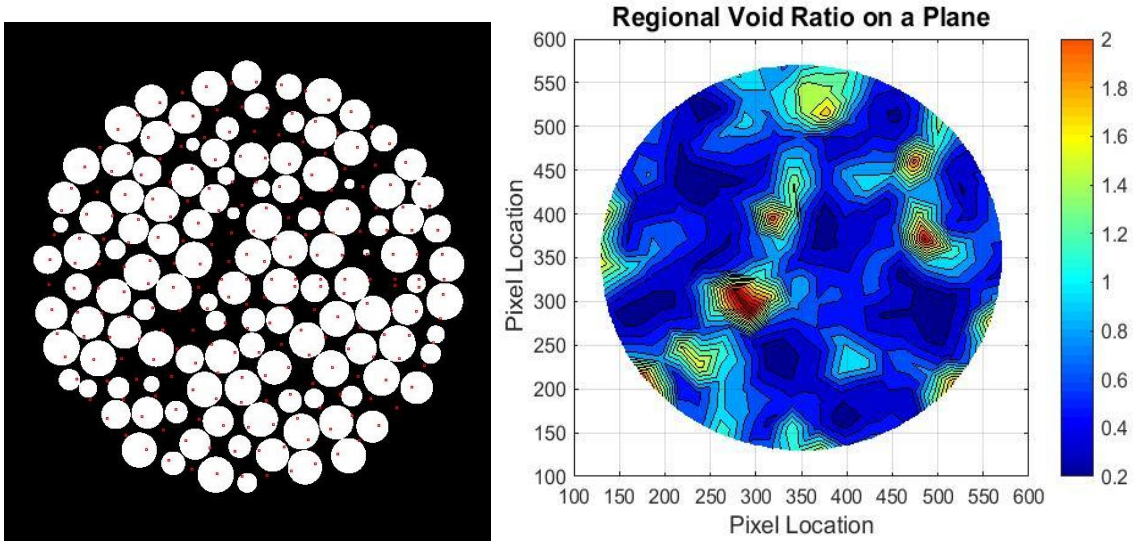

Figure 53: Center of Control Areas (Left) and Regional Void Ratio Variation (Right) at 120 mm from the Bottom of Sample Created by Radius Expansion Method

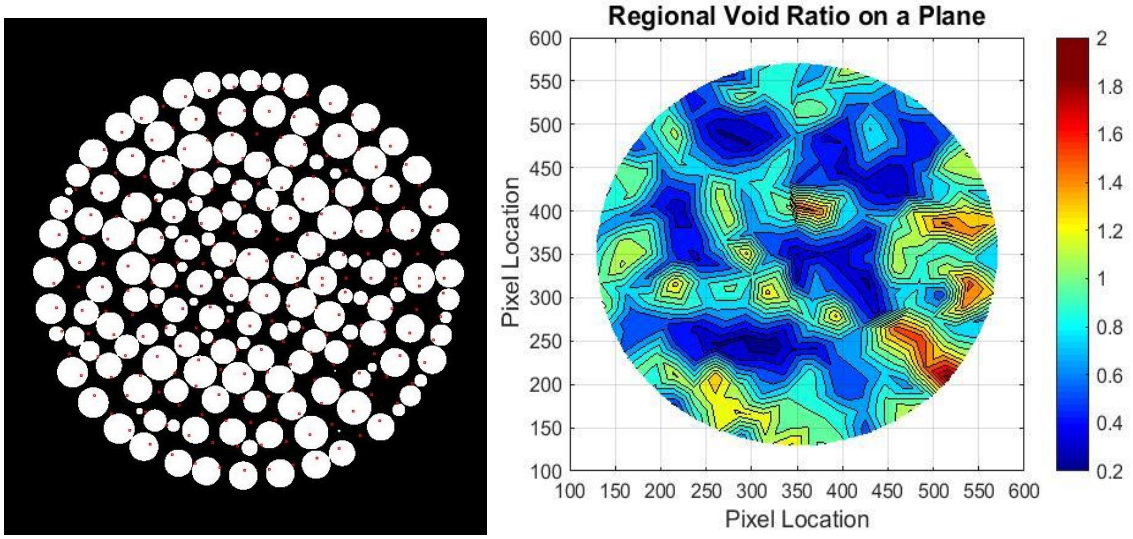

Figure 54: Center of Control Areas (Left) and Regional Void Ratio Variation (Right) at 10 mm from the Bottom of Sample Created by Air Pluviation Method

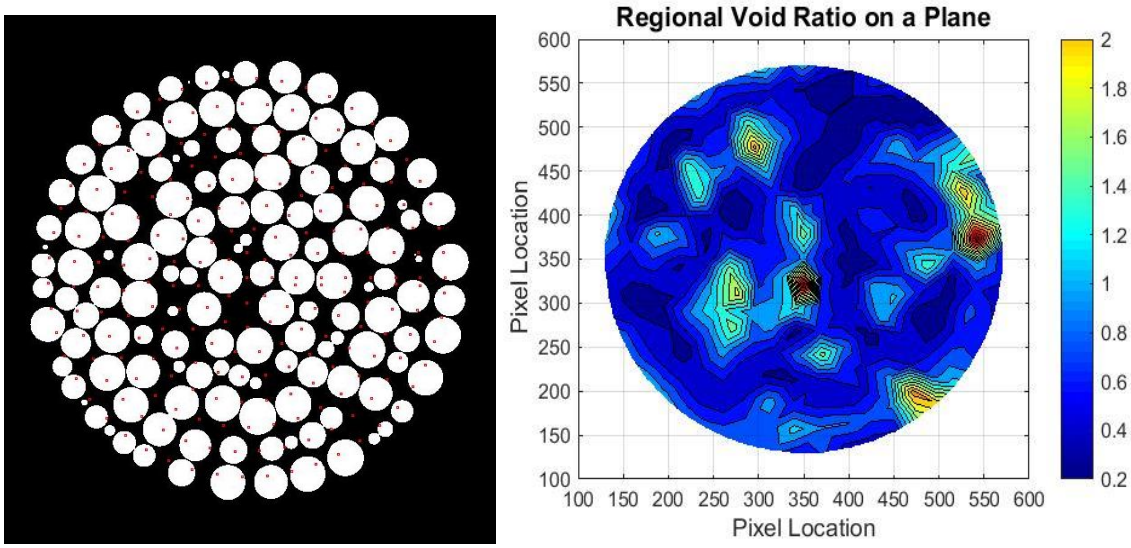

Figure 55: Center of Control Areas (Left) and Regional Void Ratio Variation (Right) at 40 mm from the Bottom of Sample Created by Air Pluviation Method

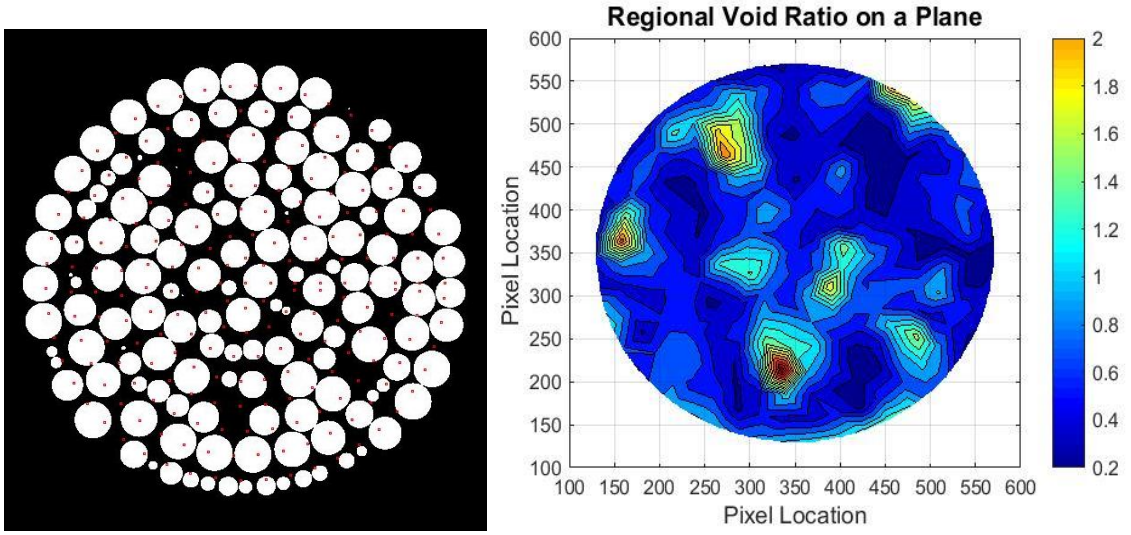

Figure 56: Center of Control Areas (Left) and Regional Void Ratio Variation (Right) at 80 mm from the Bottom of Sample Created by Air Pluviation Method

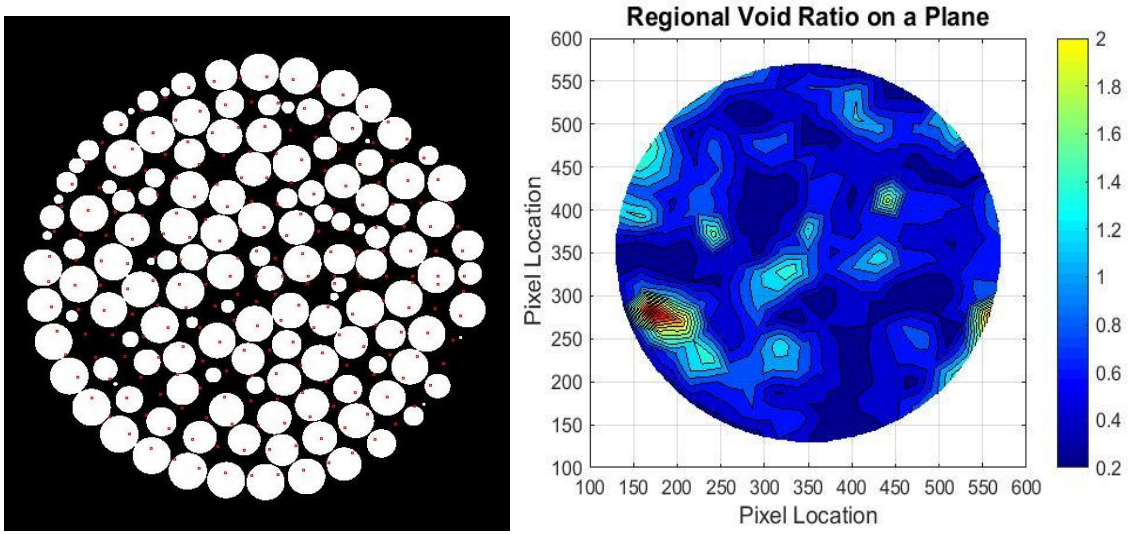

Figure 57: Center of Control Areas (Left) and Regional Void Ratio Variation (Right) at 120 mm from the Bottom of Sample Created by Air Pluviation Method

It is observed that the particle arrangement of the sample prepared by radius expansion method greatly varied within each slice. Packing of the balls is tighter for bottom slices, 10 mm and 40 mm from the bottom of the sample, and concentrated toward the center of the cross section. Moving up to the top, the packing becomes more random and more void spaces toward the center of the cross section. On the other hand, sample prepared by air pluviation method seems to have better distribution of the balls across the area. The furthest balls from the center forms an even distributed circular circumference shaped by the mold. The packing of balls for the cross section 10 mm from the bottom is the tightest. Going up to the top of the sample, void spaces within the balls also increase.

It's noteworthy that the contour plots of the regional void ratio are depend on the number of control areas defined and the size of the control areas by changing the multiple factor. More control areas defined provide more void ratio across the area. The contour

area of the sample with lower multiple factor is also smaller than the contour area of the sample with higher multiple factor. Figure 58 to 61 illustrate the difference in void ratio contour plot for multiple factor of 9 and 6 respectively. Figure 62 shows the number of control areas for multiple factor of 9 and 6 respectively.

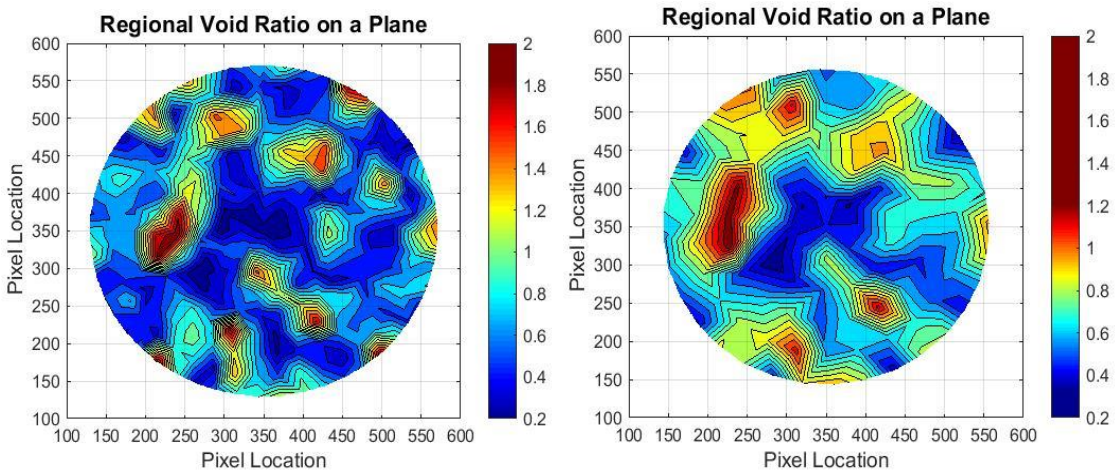

Figure 58: Contour Plots of Sample for Multiple Factor of 9 (Left) and 6 (Right) at 10 mm from the Bottom

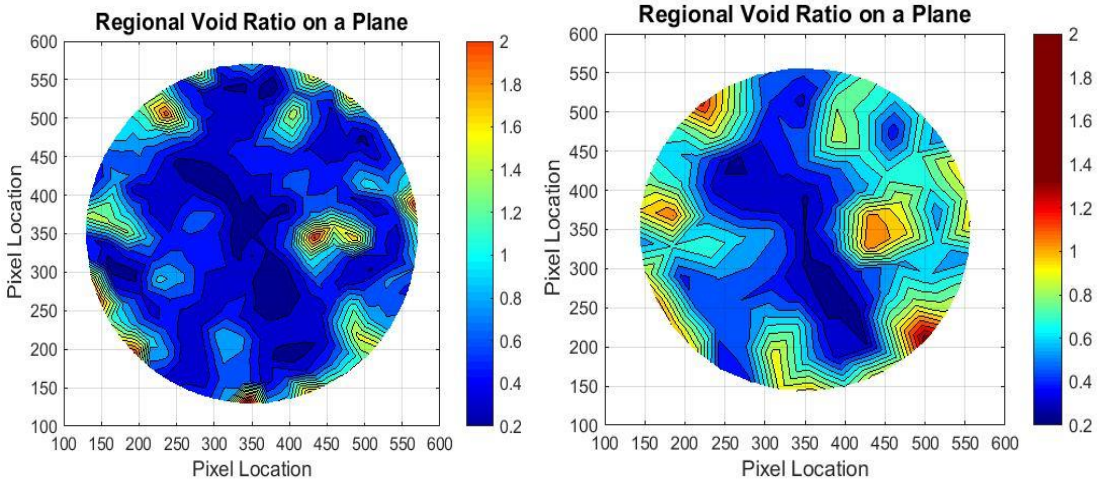

Figure 59: Contour Plots of Sample for Multiple Factor of 9 (Left) and 6 (Right) at 40 mm from the Bottom

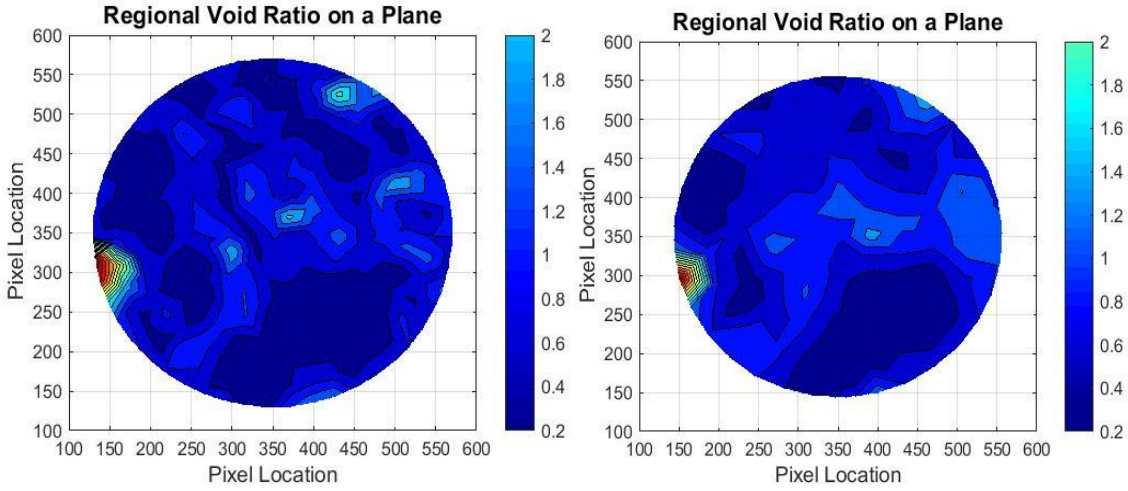

Figure 60: Contour Plots of Sample for Multiple Factor of 9 (Left) and 6 (Right) at 80 mm from the Bottom

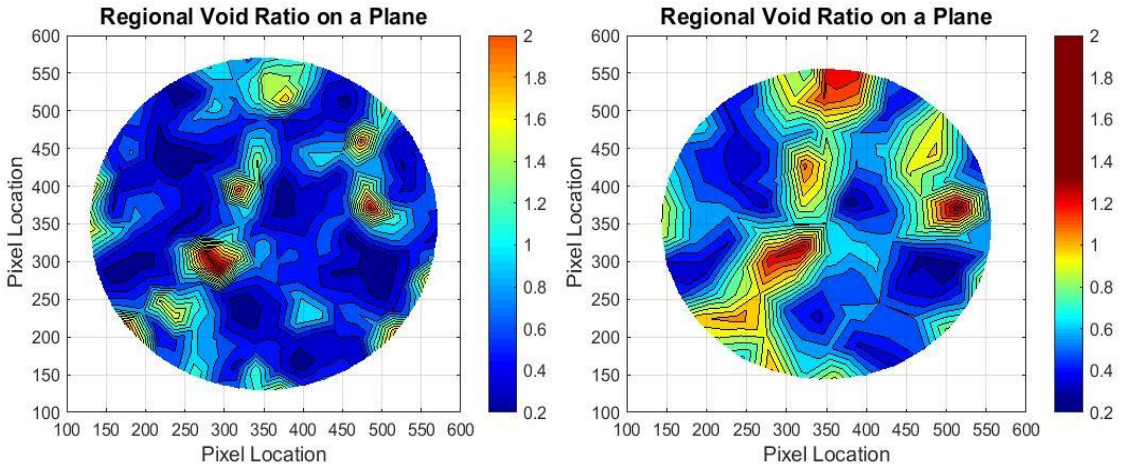

Figure 61: Contour Plots of Sample for Multiple Factor of 9 (Left) and 6 (Right) at 120 mm from the Bottom

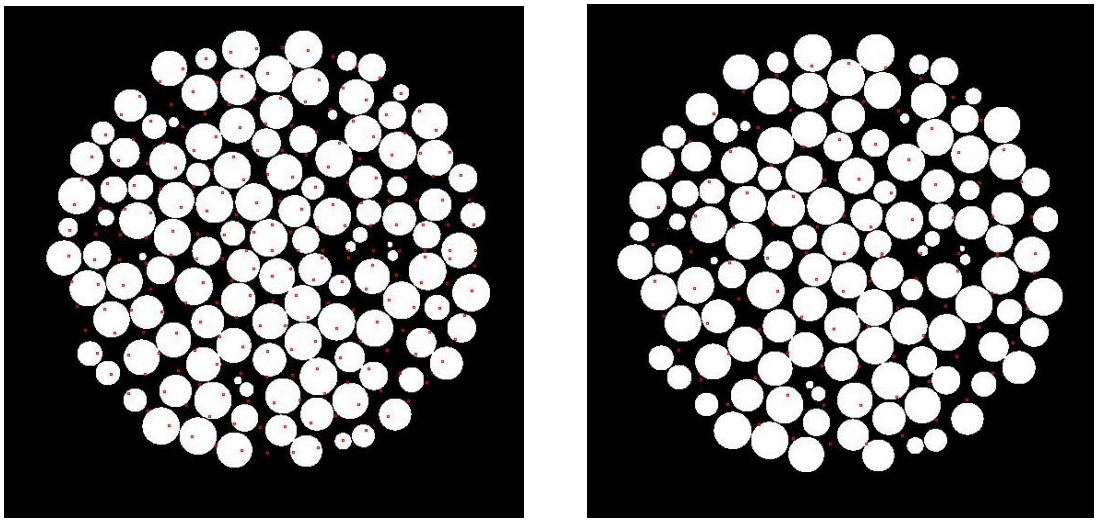

Figure 62: Centers of Control Areas for Multiple Factor of 9 (Left) and 6 (Right) at 10 mm from the Bottom

CHAPTER VII

CONCLUSION

7.1 Research Summaray

In order to assess a metric of the heterogeneity of a triaxial specimen using single diameter particles, prepared following standard procedure for constitutive homogeneous specimen, the sample preparation method called air pluviation was used. Series of samples were prepared at different particle sizes, drop heights and number of sieves placed on top of the fall tube. The void ratio of the samples increased as particle size increased (due to more void spaces created throughout the sample), increased as number of sieves increased (due to energy loss as the spheres in contact with the sieves), and decreased as drop height increased (due to higher potential energy of the spheres). Videos capturing the sample preparation process were analyzed to obtain flow velocity as the spheres enter the tube and for later comparison with the numerical model. To determine the spatial variability of the samples, x-rays computed tomography was used to capture the internal particle structure of sample. Due to the beam hardening effect, CT scan images were generated with significant amount of noise, thus further digital image analysis was not further proceeded. Prepared samples of each experimental design condition were subjected to triaxial compression test to capture the effect of sample preparation to the failure mechanism of the material. Stress-strain curves of the samples were used to compare between different sample preparation conditions.

Discrete element models generating homogeneous specimens were built using PFC3D program. Two methods of generating specimens, the radius expansion method and the air pluviation method were compared. Different methods to examine the spatial variability of void ratio were considered, PFC measurement spheres, planar void ratio variation and regional void ratio variation on a plane. Since the experiment data was unavailable, no direct comparison between experiment and numerical model spatial void ratio variation were performed. Spatial void ratio variation were compared between two methods of generating PFC specimens. Planar void ratio analysis showed PFC model replicating air pluviation process generated average planar void ratio closer to the experimental global void ratio than PFC model using radius expansion method. In the regional void ratio analysis of a plane, air pluviation method provided better particle evenly distribution across the plane. Due to time limitation, only 4 samples prepared by radius expansion method were subjected to triaxial compression. The difference in stress-strain response might be caused by inaccurate specification of strain rate.

7.2 Future Study

The aim is to improve and expend the investigation of the heterogeneity of the samples can achieve by obtaining better quality X-rays CT scan images of the samples to have direct comparison between experimental and numerical simulation results. Possible options are to look for different materials with lower density than chrome steel to reduce beam hardening effect or to look for available X-rays CT scan machine that is configured to take images of geomaterial samples.

Detailed analysis of the effect of sample preparation condition to sample failure mechanism can be achieve by performing more triaxial compression test for each condition to prepare samples both experimentally and numerically. Simulation of the triaxial compression for samples prepared by air pluviation method should be performed to compare with samples prepared by radius expansion method and experiment results. Better numerical simulation results can obtain by performing parametric analysis on factors that affect material behaviors including loading rate, and choice of contact model.

Furthermore, the parametric analysis of factors that affect computational effort for each PFC model should be investigated to improve computational efficient. Especially the computational time for sample preparation replicating air pluviation process should be reduced.

In addition, it is beneficial to introduce the effect of grain size distribution on the heterogeneity of the samples and their failure mechanism by mixing two particle sizes, 3 mm and 6 mm diameter. Smaller grains will fill the void spaces created by the larger grains. The samples are then subjected to triaxial compression. Numerical simulation of the samples shall be performed as well.

A multiphysics approach can also be analyzed by introducing pore pressure to the sample experimentally and numerically. A possible option to simulate the effect of pore water pressure is coupling the discrete element model with a finite element program such as FLAC or ABAQUS. By achieving this, complex geotechnical field tests such as cone penetration test can be replicated in PFC.

REFERENCES

[1] Oda M. Initial Fabrics and Their Relations to Mechanical Properties of Granular Material. Soils Foundation 1972; 12(1): 17-35.

[2] Arthur JRF and Menzies BK. Inherent Anisotropy in A Sand. Geotechnique 1972; 22(1): 115-128.

[3] Ladd RS. Specimen Preparation Method and Liquefaction of Sands. Journal of the Geotechnical Engineering Division 1974; 100(10): 1180-1184.

[4] Mulilis JP, Seed HB, Chan CK, Mitchell JK, and Arulanandan K. Effects of Sample Preparation on Sand Liquefaction. Journal of Geotechnical Engineering Division 1977; 103(2): 91-108.

[5] Sadrekarimi A and Olson MS. Effect of Sample-Preparation Method on Critical-State Behavior of Sands. Geotechnical Testing Journal 2012; 35(4). DOI: 10.1520/GTJ104317.

[6] Viad YP, Sivathayalan S, and Stedman D. Influence of Specimen-Reconstituting Method on the Undrained Response of Sand. Geotechnical Testing Journal 1999; 22(3): 187-195.

[7] Yammamuro JA, Wood FM, and Lade PV. Effect of Depositional Method on the Microstructure of Silty Sand. Canadian Geotechnical Journal 2008; 45: 1538-1555.

[8] Thomson PR and Wong RCK. Specimen Nonuniformities in Water-Pluviated and Moist-Tamped Sands under Undrained Triaxial Compression and Extension. Canadian Geotechnical Journal 2008; 45(7): 939-956.

[9] Itasca Consulting Group. PFC3D (Particle Flow Code in Three-Dimensions). Version 5.0. Minneapolis (MN): 2014.

[10] Tao H, Jin B, Zhong W, Wang X, Ren B, Zhang Y, and Xiao R. Discrete Element Method Modeling of Non-Spherical Granular Flow in Rectangular Hopper. Chemical Eningeering and Processing 2010; 49: 151-58.

[11] Yin Wang and Jin Y Ooi. A Study of Granular Flow in a Conical Hopper Discharge Using Discrete and Continuum Approach. Procedia Engineering 2015; 102: 765-772.

[12] Lu M and McDowell GR. Discrete Element Modeling of Railway Ballast Under Monotonic and Cyclic Triaxial Loading. Geotechnique 2010; 60: 459-67.

[13] Wu J, Collop AC, and McDowell GR. Discrete Element Modeling of Constant Strain Rate Compression Tests on Idealized Asphalt Mixture. Journal of Materials in Civil Engineering 2011; 23(1): 2-11.

[14] Potyondy DO and Cundall PA. A Bonded-Particle Model for Rock. International Journal of Rock Mechanics & Mining Sciences 2004; 41: 1329-364.

[15] Parker MB. Simulation and Analysis of Particle Flow through an Aggregate Stockpile. [M.S. Thesis]. Blacksburg (VA): Virginia Polytechnic Institute; 2009.

[16] Hou YL, Zhou YD, and Zhang CH. Numerical Simulation of Arch Dam Failure by 3D Deformable Distinct Element Method. Frontiers of Discontinuous Numerical Methods and Practical Simulations in Engineering and Disaster Prevention. CRC Press 2013; 443-449.

[17] Preh A. PFC3D Application. The Akenes/Tafjord project. 2007. Available: http://folk.uio.no/geirkp/Aaknes/.

[18] Cundall PA and Strack ODL. A Discrete Numerical Model for Granular Assemblies. Geotechnique 1979; 29: 47-65.

[19] Medina-Cetina Z. Probabilistic Calibration of Soil Constitutive Models. [Ph.D. Dissertation]. Baltimore (MD): The Johns Hopkins University; 2007.

[20] Medina-Cetina Z and Khoa HDV, Probabilistic Calibration of Discrete Particle Models for Geomaterials. ISSMFE conference, Egypt. 2009.

[21] Sullivan CO. Micromechanics of Granular Materials Response during Load Reversal: Combined DEM and Experimental Study. Power Technology 2009; 193: 289-302.

[22] Yanbei Z. Probabilistic Calibration of a Discrete Particle Model. [M.S. Thesis]. College Station (TX): Texas A&M University; 2010.

[23] Bloom M, Russell MJ, Kustau A, Mandayam S, and Sukumaran B. Measurement of Porosity in Granular Particle Distributions Using Adaptive Thresholding. Instrumentation and Measurement, IEEE Transactions 2010; 59(5): 1192-1199.

[24] Yimsiri S and Soga K. Effects of Soil Fabric on Behavior of Granular Soil: Microscopic Modeling. Elsevier 2011.

[25] Noble PA. Uncertainty Quantification of the Homogeneity of Granular Materials Through Discrete Element Modeling and X-rays Computed Tomography. [M.S. Thesis]. College Station (TX): Texas A&M University; 2012.

[26] Hill JM and Selvadurai APS. Mathematics and Mechanics of Granular Materials. Journal of Engineering Mathematics 2005; 52: 1-9.

[27] Zhu HP, Zhou ZY, Yang RY, and Yu AB. Discrete Particle Simulation of Particulate Systems: Theoretical Developments. Chemical Engineering Science 2007; 62(13): 3378-3396.

[28] Zhu HP, Zhou ZY, Yang RY, and Yu AB. Discrete Particle Simulation of Particulate Systems: A Review of Major Applications and Findings. Chemical Engineering Science 2008; 63(23): 5728-5770.

[29] Sullivan CO. Particle-Based Discrete Element Modeling: Geomechanics Perspective. International Journal of Geomechanics 2011; 11(6): 449-464.

[30] Precision Ball Product Catalog, Thomson, 2010. Available: http://www.thomsonprecisionball.com/images/pdfs/PrecisionBalls-9-26-08_loRes.pdf.

[31] Brown D. Tracker-Video Analysis and Modeling Tool. 2013. Available: http://www.cabrillo.edu/~dbrown/tracker/.

[32] ASTM Standard D2850. Standard Test Method for Unconsolidated-Undrained Triaxial Compression Test on Cohesive Soils. ASTM International, West Conshohocken, PA, 2007, DOI: 10.1520/D2850-03AR07, www.astm.org.

[33] National Instruments. LabView. 2012. Available: http://www.ni.com/labview.

[34] MathWorks. MATLAB – The Language of Technical Computing [Computer Program on Disk]. Version 8.4.0. Natick (MA): 2014.

[35] Itasca. PFC3D 5.0 Manual. Particles Flow Code in three dimensions-PFC3D. 2014. Available: http://www.itascacg.com/pfc3d.

[36] Potyondy D. Material-Modeling Support in PFC. Technical Memorandum ICG7766-L. Itasca Consulting Group. Minneapolis (MN): 2015.

APPENDIX

Sample preparation: Air Pluviation Method

Purpose: to generate a homogeneous cylindrical sample composed of granular material

Procedure:

1. Prepare the mold, place a porous stone in the bottom and cover with a membrane
2. Use double o-rings in the bottom to seal the void from getting out of the membrane
3. Install the mold and tighten it with double metal rings
4. Apply vacuum pressure on both sides of the mold
5. Use one o-ring on top of the mold to straighten & locate the position of the membrane
6. Place an acrylic tube with preferred choice of height on top of the mold
7. Place the sieve(s) on top of the tube
8. Pour all the balls into a closed end funnel
9. Release balls from the funnel at a constant height above the top sieve
10. Check the velocity of falling of the balls
11. Discard the exceed balls on top of the mold using a ruler
12. Put a porous stone and a plastic cap on top of the sample
13. Slowly roll up the top o-ring onto a section of acrylic tube to prevent disturbance to the top section of the sample
14. Slowly roll up the top part of the membrane
15. Transfer the o-ring to the bottom part of the sieve
16. Carefully seal the top of the sample
17. Check if vacuum pressure is constant (before ejecting pressure from both sides of the mold and re-injecting pressure from below), if not, check for holes on membrane. Record the pressure
18. Sample should be perfectly cylindrical (no necking)
19. Carefully measure the height (5 times) and diameter (10 times) of the sample
20. Weight the sample (if not performing the triaxial test)

Notes:

- The height from the top sieve to where the ball is released should be constant
- Use a camera to capture the fall of spheres and use a program to analyze the velocity of the ball
- Replace the membrane after ~10 times of uses